Nonlinear shallow-water oscillations in a parabolic channel: exact solutions and trajectory analyses

By ALAN SHAPIRO

Center for Analysis and Prediction of Storms, University of Oklahoma, Norman, OK 73019, USA

A new exact solution of the nonlinear shallow-water equations is presented. The solution corresponds to divergent and non-divergent free oscillations in an infinite straight channel of parabolic cross-section on the rotating Earth. It provides a description of the one-dimensional subclass of shallow-water flows in paraboloidal basins considered by Ball (1964), Thacker (1981), Cushman-Roisin (1987) and others in which the velocity field varies linearly and the free-surface displacement varies quadratically with the spatial coordinates. In contrast to the previous exact solutions describing divergent oscillations in circular and elliptic paraboloidal basins, the oscillation frequency of the divergent oscillation in the parabolic channel is found to depend, in part, on the amplitudes of the relative vorticity and free-surface curvature. This result is consistent with Thacker's (1981) numerical finding that when the free surface in parabolic channel flow is curved, the oscillation frequency depends on the amplitude of the motion. Solutions for parcel trajectories are also presented. The exact solution provides a rare description of a class of nonlinear flows and is potentially valuable as a validation test for numerical shallow-water models in Eulerian and Lagrangian frameworks.

1. Introduction

Despite the fundamental role of shallow-water theory in atmospheric, oceanographic and engineering flow problems, few exact solutions have been obtained. The primary difficulty in obtaining analytic solutions stems from the presence of nonlinear terms associated with fluid inertia, terms that render conventional (i.e. linear) analysis techniques powerless in the general case. One of the classic solutions in shallow-water theory is the dam break solution of the shallow-water equations (Whitham 1974; Stoker 1958). Another well-known solution describes the propagation of shallow-water waves up a sloping beach (Carrier & Greenspan 1958). These and other exact solutions in shallow-water theory are of theoretical interest in their own right and are also potentially useful as test solutions for the validation of numerical models of tides, seiches and storm surges.

Presented herein is an exact analytic solution for a class of finite-amplitude inviscid shallow-water oscillations in an infinite straight channel of parabolic cross-section. Provision is made for the Earth's rotation with a constant Coriolis parameter. The shoreline, a moving boundary, is determined as part of the solution. The solution is a member of a class of shallow-water flows characterized by a velocity field that varies linearly and a free-surface displacement that varies quadratically with the spatial coordinates. These restrictions reduce the shallow-water equations, without approximation, to a finite set of nonlinear coupled ordinary differential equations.

Analytic solutions to these ordinary differential equations have been found in special circumstances by several investigators but the most general solution has yet to be obtained.

Goldsbrough (1931) showed that the spatial structure of linear free oscillations in a non-rotating elliptic basin having a paraboloidal depth variation could be described by low-order polynomials. Some three decades later, Ball (1963) recognized that low-order polynomials (linear for velocity, quadratic for free-surface displacement) could also describe nonlinear shallow-water oscillations in paraboloidal basins, with or without a rotating framework. Subsequent investigations by Miles & Ball (1963), Ball (1964, 1965), Thacker (1981), Cushman-Roisin (1984, 1987) and Cushman-Roisin, Heil & Nof (1985) extended the exact solutions of the nonlinear flows constrained by this spatial structure. Thacker described these flows as nonlinear normal mode oscillations of shallow water in paraboloidal basins. As such, they may be of relevance to free oscillations in lakes, channels and gulfs. Cushman-Roisin applied his elliptical vortex solution to oceanic warm-core rings. Numerical solutions of the forced (two-level) and unforced system were employed by Tsonis *et al.* (1994) in a study of nonlinear time series analyses. Solutions to the forced system exhibited chaotic properties. Although the unforced system did not exhibit chaotic properties, the solutions could be quite complicated for certain parameter choices.

In the next section we formulate the problem of the one-dimensional subclass of these flows in which the basin is a channel and the fluid moves in both the along-channel and cross-channel directions but with no variation in the along-channel direction. The free-surface displacement is composed of divergent and non-divergent components. The pure non-divergent mode is examined in §3. Integrals of motion for the general case are derived in §4. In §5 we deduce the oscillatory behaviour of the divergent mode and present the exact solution. The frequency of the divergent oscillation is a function of two non-dimensional governing parameters involving the basin geometry, the Coriolis parameter, the relative vorticity and the curvature of the free-surface. This result is consistent with the numerical finding reported by Thacker (1981) that when the free surface is curved, the frequency of oscillations in the channel depends on the amplitude of the motion. In §6 we summarize the solution to the initial value problem. Analytic parcel trajectories are derived in §7. Specific examples are examined in §8.

2. Formulation

Consider inviscid shallow-water flow in a channel where the free surface and velocity field are independent of the along-channel coordinate. The equations of motion and mass conservation for these flows are

$$\frac{\partial u}{\partial t} + u\frac{\partial u}{\partial x} - fv + g\frac{\partial h}{\partial x} = 0, \tag{1}$$

$$\frac{\partial v}{\partial t} + u\frac{\partial v}{\partial x} + fu = 0, \tag{2}$$

$$\frac{\partial h}{\partial t} + \frac{\partial}{\partial x}[u(D+h)] = 0, \tag{3}$$

where x and y are the Cartesian coordinates in the cross- and along-channel directions, respectively, u and v are the Cartesian velocity components in the cross- and along-channel directions, respectively, f is the Coriolis parameter (assumed constant), and g
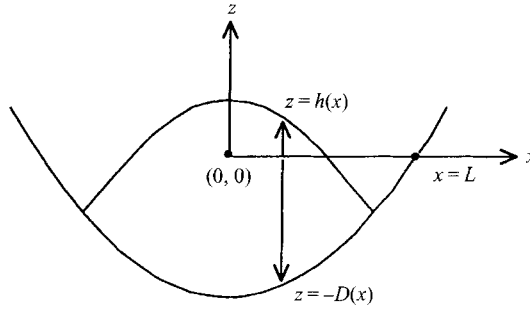
FIGURE 1. Definitional sketch for one-dimensional shallow-water flow in a straight channel of parabolic depth variation $D(x) = D_0(1 - x^2/L^2)$. The free-surface displacement $h(x, t)$ and the velocity field are independent of the along-channel (y) coordinate.

is the acceleration due to gravity (or a reduced-gravity constant). The channel depth $D(x)$ is reckoned positive beneath $z = 0$ (i.e. $z = -D(x)$ defines the channel topography), and the free-surface displacement $h(x, t)$ is reckoned positive above $z = 0$, so the total fluid depth is $D(x) + h(x, t)$. The values of x for which $D(x) + h(x, t) = 0$ mark the intersection of the free surface with the channel and define the location of the moving shoreline. A definitional sketch is provided in figure 1.

Several useful integral constraints (invariants of motion) can be derived for the one-dimensional shallow-water system (1)–(3) assuming the lateral extent of the flow is finite. Denoting the western and eastern time-dependent shorelines by $r_-(t)$ and $r_+(t)$, respectively, we can write conservation equations for the integrated energy and mass (per unit y-length) in the channel as

$$\int_{r_-}^{r_+} \partial/\partial t\,[(D+h)(u^2+v^2)/2 + g(h^2-D^2)/2]\,dx = 0 \quad \text{and} \quad \int_{r_-}^{r_+} \partial/\partial t(D+h)\,dx = 0.$$

Interchanging the order of differentiation and integration in these constraints (a legitimate step since $D+h$ vanishes at the shoreline), we find that

$$\int_{r_-}^{r_+} (D+h)\,dx = M \quad \text{and} \quad \int_{r_-}^{r_+} [(D+h)(u^2+v^2)/2 + g(h^2-D^2)/2]\,dx = E,$$

where M and E are independent of time. It can also be shown that the integrated absolute y-momentum

$$\int_{r_-}^{r_+} (D+h)(v+fx)\,dx$$

and integrated absolute vertical vorticity

$$\int_{r_-}^{r_+} (\partial v/\partial x + f)\,dx$$

are independent of time. More generally, it can be shown that since the potential vorticity $Q \equiv (\partial v/\partial x + f)/(D+h)$ is conserved following fluid motion; that is

$$\frac{\partial Q}{\partial t} + u\frac{\partial Q}{\partial x} = 0, \quad \int_{r_-}^{r_+} (D+h)\,F(Q)\,dx$$

must be independent of time, where F is an arbitrary function of Q.

We seek special solutions of (1)–(3) for which the x-coordinate dependences of the free-surface displacement, channel depth and velocity field are described by low-order polynomials (quadratic for h and D and linear for u and v). Adopting Thacker's (1981) notation, we write the free-surface displacement and channel geometry in the form†

$$h(x,t) = h_0(t) + h_x(t)\,x + \tfrac{1}{2}h_{xx}(t)\,x^2, \quad D(x) = D_0(1 - x^2/L^2), \tag{4}$$

with the velocity field varying as

$$u(x,t) = u_0(t) + u_x(t)\,x, \quad v(x,t) = v_0(t) + v_x(t)\,x. \tag{5}$$

If the centreline channel depth $D_0 (\equiv D(0))$ is positive the topography is a channel of parabolic cross-section; if $D_0 = 0$ the flow takes place over a horizontal surface, and if $D_0 < 0$ the flow takes place over a parabolic ridge. For the first case, $D_0 > 0$, we assume that the total fluid mass is not only conserved, but is (i) finite (per unit y-length) and (ii) equal to the mass in an undisturbed channel with a planar free surface at $z = 0$ (the equilibrium free surface in a non-rotating channel). For $D_0 = 0$ and $D_0 < 0$ we are mostly concerned with cases where the total fluid mass is finite (per unit y-length), for example, where a parabolic ridge of fluid is situated on top of a parabolic ridge of lesser convex curvature.

In view of (5), the horizontal divergence $\partial u/\partial x + \partial v/\partial y$ is equal to $u_x(t)$, while the relative vorticity $\partial v/\partial x - \partial u/\partial y$ is equal to $v_x(t)$. Thus, the divergence and vorticity fields are spatially constant and the advection terms must vanish from their respective evolution equations.

Before considering other dynamical implications of (4) and (5), we note some simple geometrical implications. The transformations $x' \equiv x + h_x/h_{xx}$ and $h'_0 \equiv h_0 - h_x^2/(2h_{xx})$ remove the h_x term from the free-surface displacement, resulting in $h = h_{xx} x'^2/2 + h'_0$. Thus, the free surface is a parabola of (instantaneous) curvature h_{xx} displaced horizontally by a factor of h_x/h_{xx} and vertically by a factor of $h_x^2/(2h_{xx})$. Also note that the fluid depth as $x \to \pm \infty$ depends on the difference between the free-surface curvature h_{xx} and the curvature of the channel $2D_0/L^2$. If $h_{xx} - 2D_0/L^2 > 0$ the fluid depth is positive and unbounded as $x \to \pm \infty$. If $h_{xx} - 2D_0/L^2 < 0$ the fluid depth becomes negative for large x and the fluid is confined to a finite part of the x-domain where $D + h$ is positive. In this investigation we are concerned primarily with the latter case of finite fluid mass (per unit y-length).

Applying (4) and (5) to (1)–(3) and collecting terms in common powers of x, results in a system of seven coupled nonlinear ordinary differential equations in seven unknowns:

$$du_0/dt + u_0 u_x - fv_0 + gh_x = 0, \tag{6}$$

$$du_x/dt + u_x^2 - fv_x + gh_{xx} = 0, \tag{7}$$

$$dv_0/dt + u_0(v_x + f) = 0, \tag{8}$$

$$dv_x/dt + u_x(v_x + f) = 0, \tag{9}$$

$$dh_0/dt + u_x(D_0 + h_0) + u_0 h_x = 0, \tag{10}$$

$$dh_x/dt + 2u_x h_x + u_0(h_{xx} - 2D_0/L^2) = 0, \tag{11}$$

$$dh_{xx}/dt + 3u_x(h_{xx} - 2D_0/L^2) = 0. \tag{12}$$

In contrast to low-order systems that are truncated expansions (approximations) of partial differential equations (e.g. the Lorenz equations), our system of ordinary

---

† As noted by Thacker (1981), inclusion of a linear term for D amounts to a shift in coordinates (a linear term could be removed from D by a change of variable, leaving the form of h unchanged). We have therefore excluded such a term at the outset.

differential equations follows from the original partial differential equations (1)–(3) without approximation. The fact that our original equation set reduces to a finite set of ordinary differential equations verifies that exact solutions of the shallow-water equations of the form (4) and (5) are at least mathematically feasible. Of course, whether such flows can be realized in practice depends, in part, on the stability of these solutions, an issue that is beyond the scope of the present investigation.

Equations (7), (9) and (12) comprise a sub-system of three equations in the three unknowns v_x, u_x and h_{xx} and can be solved independently of the other equations. These three variables interact with each other and also serve as external forcings in the equations for u_0, v_0, h_0 and h_x. The variables v_x, u_x and h_{xx} comprise a divergent mode while u_0, v_0, h_0 and h_x comprise a non-divergent mode. Since (10) is the only equation involving h_0, we can compute h_0 as a residual once the other variables have been obtained.

3. Steady-state solutions: pure non-divergent mode

The trivial state of no motion is a solution of (6)–(12). To derive other steady states, we set the time derivatives in (6)–(12) to zero. Examination of (12) then shows that $u_x = 0$ and/or $h_{xx} = 2D_0/L^2$. If $u_x \neq 0$ we find by working upward from (12) to (10) that $h_{xx} = 2D_0/L^2$, $h_x = 0$, and $D_0 + h_0 = 0$; so $D + h = 0$ for all x. Since there would be no fluid in this case, our assumption that $u_x \neq 0$ is not tenable and u_x must be zero. Equations (6) and (7) then yield the geostrophic relations, $h_x = fv_0/g$, and $h_{xx} = fv_x/g$, while equations (8), (10) and (11) reveal that either (i) $u_0 = 0$ or (ii) $v_x + f = 0$, $h_x = 0$, and $h_{xx} = 2D_0/L^2$. In case (i) we obtain

$$u_0 = u_x = 0, \quad h_x = fv_0/g, \quad h_{xx} = fv_x/g, \left.\begin{array}{c} \\ \\ \end{array}\right\} \qquad (13)$$
$$v_0, v_x \quad \text{and} \quad h_0 \text{ are arbitrary constants,}$$

whereas in case (ii), h_0 and u_0 are arbitrary constants and h_{xx} is equal to both $-f^2/g$ and $2D_0/L^2$. Thus, the fluid depth is of uniform thickness, $D + h = D_0 + h_0$, and $D_0 = -L^2 f^2/(2g)$. If $f = 0$ ($D_0 = 0$) the free surface is horizontal and we obtain uniform flow on a non-rotating horizontal plane:

$$h_0, u_0 \quad \text{and} \quad v_0 \text{ are arbitrary constants,} \left.\begin{array}{c} \\ \\ \end{array}\right\} \qquad (14)$$
$$h_x = h_{xx} = v_x = u_x = 0,$$

whereas if $f \neq 0$ (so $D_0 = -L^2 f^2/(2g) < 0$), the flow takes place over a ridge,

$$h_0 \quad \text{and} \quad u_0 \text{ are arbitrary constants,} \left.\begin{array}{c} \\ \\ \\ \end{array}\right\}$$
$$v_x = -f, \quad h_{xx} = \frac{2D_0}{L^2}\left(= -\frac{f^2}{g}\right), \quad v_0 = h_x = u_x = 0. \qquad (15)$$

Now suppose that only the divergent mode variables v_x, u_x and h_{xx} are in a steady state. It can be shown that $u_x = 0$ (as in the previous case), $v_x = c$, a constant, $h_{xx} = fv_x/g$, and

$$\mathrm{d}u_0/\mathrm{d}t - fv_0 + gh_x = 0, \qquad (16)$$

$$\mathrm{d}v_0/\mathrm{d}t + u_0(c + f) = 0, \qquad (17)$$

$$\frac{\mathrm{d}h_x}{\mathrm{d}t} + u_0\left(\frac{fc}{g} - \frac{2D_0}{L^2}\right) = 0, \qquad (18)$$

$$\mathrm{d}h_0/\mathrm{d}t + u_0 h_x = 0. \qquad (19)$$

Differentiating (16) and making use of (17) and (18) results in $d^2u_0/dt^2 + Bu_0 = 0$, where $B \equiv f^2 + 2gD_0/L^2$. After solving for u_0, integrate (17), (18) and (19) in turn to obtain v_0, h_x and h_0. The form of the solutions depends on the sign of B. If $B = 0$, a parabolic blob or infinite wedge of fluid accelerates over a horizontal plane ($D_0 = 0$, $f = 0$) or over a ridge ($D_0 = -L^2f^2/(2g) < 0$),

$$u_x = 0, \quad v_x = c, \quad u_0 = a + bt, \quad v_0 = -(c+f)(at + \tfrac{1}{2}bt^2) + d, \quad (20a\text{--}d)$$

$$h_x = -\frac{f}{g}(c+f)(at + \tfrac{1}{2}bt^2) + \frac{fd-b}{g}, \quad h_{xx} = \frac{fv_x}{g}, \quad (20e,f)$$

$$h_0 = \frac{f}{2g}(c+f)t^2(a + \tfrac{1}{2}bt)^2 + \frac{b-fd}{g}(at + \tfrac{1}{2}bt^2) + e, \quad (20g)$$

where a, b, c, d and e are integration constants. If $B > 0$ ($D_0 > -L^2f^2/(2g)$) we obtain inertia–gravity waves in a channel ($D_0 > 0$), on a flat plane ($D_0 = 0$) or over a ridge ($D_0 < 0$),

$$u_x = 0, \quad v_x = c, \quad u_0 = a\cos(B^{1/2}t - b), \quad v_0 = -\frac{a(c+f)}{B^{1/2}}\sin(B^{1/2}t - b) + d,$$
$$(21a\text{--}d)$$

$$h_x = -\frac{a}{B^{1/2}}\left(\frac{fc}{g} - \frac{2D_0}{L^2}\right)\sin(B^{1/2}t - b) + \frac{fd}{g}, \quad h_{xx} = \frac{fv_x}{g}, \quad (21e,f)$$

$$h_0 = -\frac{a^2}{4B}\left(\frac{fc}{g} - \frac{2D_0}{L^2}\right)\cos[2(B^{1/2}t - b)] - \frac{fda}{gB^{1/2}}\sin(B^{1/2}t - b) + e. \quad (21g)$$

The non-divergent components of the velocity field oscillate with a period of $2\pi/B^{1/2}$. The free-surface oscillation is composed of two periods: $2\pi/B^{1/2}$ and $\pi/B^{1/2}$, the latter periodicity arising from nonlinear terms. This flow is equivalent to Thacker's (1981) equation (33) if there is no wind shear ($c = 0$) and no mean pressure gradient ($d = 0$).

If $B < 0$ ($D_0 < -L^2f^2/(2g) \leqslant 0$), the solution is

$$u_x = 0, \quad v_x = c, \quad h_{xx} = fv_x/g, \quad (22a\text{--}c)$$
$$u_0 = a\exp((-B))^{1/2}t) + b\exp(-(-B)^{1/2}t),$$

$$v_0 = -\frac{c+f}{(-B)^{1/2}}(a\exp((-B^{1/2})t) - b\exp(-(-B^{1/2})t)) + d, \quad (22d,e)$$

$$h_x = -\frac{1}{(-B)^{1/2}}\left(\frac{fc}{g} - \frac{2D_0}{L^2}\right)[a\exp((-B)^{1/2}t) - b\exp(-(-B)^{1/2}t)] + \frac{fd}{g}, \quad (22f)$$

$$h_0 = -\frac{1}{2B}\left(\frac{fc}{g} - \frac{2D_0}{L^2}\right)[a^2\exp(2(-B)^{1/2}t) + b^2\exp(-2(-B)^{1/2}t)]$$

$$-\frac{fd}{g(-B)^{1/2}}[a\exp((-B)^{1/2}t) - b\exp(-(-B)^{1/2}t)] + e. \quad (22g)$$

With attention restricted to $fv_x < 0$ (and e large enough to ensure that the fluid depth is positive on part of the domain), the fluid mass is finite and the free surface is a parabola. If $b/a < 0$ the parabolic blob of fluid ascends part of the way up the parabolic ridge and then accelerates back down the ridge, the way it came, whereas if $b/a > 0$ the blob of fluid rises over the crest of the ridge and then accelerates down the other side. In either case, the curvature of the free surface remains constant while h_0 and h_x

become unbounded as $t \to \infty$. Presumably, these unbounded solutions might become bounded if friction is included in the governing equations. If the initial values of u_0, v_0 and h_x are such that $(-B)^{1/2} u_0 + fv_0 - gh_x = 0$ then $a = 0$ and a steady state is reached as $t \to \infty$ (if $d = 0$ the blob reaches an equilibrium position at the top of the ridge). However, any slight violation of this condition results in $a \neq 0$, so the equilibrium solutions are unstable.

In summary, oscillatory solutions for the pure non-divergent mode are found for parabolic channels of any aspect ratio and for parabolic ridges with sufficiently gentle slopes. The period of the velocity field oscillation is $2\pi/B^{1/2}$. The periods of the free-surface oscillations are $2\pi/B^{1/2}$ and $\pi/B^{1/2}$. If $D_0 < -L^2 f^2/(2g) (B < 0)$, the ridge is too steep to support waves and solutions become unbounded.

4. Integrals of motion

In the previous section we examined the solutions for which u_x, v_x and h_{xx} were stationary and found that u_x was necessarily zero. In this section we obtain integrals of (6)–(12) for the general case where u_x is not identically zero. We first consider the sub-system (7), (9) and (12) describing the divergent mode.

4.1. *Divergent mode*

Since (7) is, formally, a Riccati equation for u_x, we introduce a transformation designed to remove the quadratic nonlinearity from the Riccati equation (Davis 1962) in the hope that it will simplify the problem

$$u_x = \frac{1}{\phi} \frac{d\phi}{dt}. \tag{23}$$

Applying (23) in (9) and integrating results in

$$v_x + f = a/\phi, \tag{24}$$

where a is an integration constant. Similarly, applying (23) to (12) and integrating results in

$$h_{xx} - 2D_0/L^2 = c/\phi^3, \tag{25}$$

where c is an integration constant. Since we are restricting attention to cases where $h_{xx} - 2D_0/L^2 < 0$ (see §2), $c = 0$ is excluded from consideration.

To obtain a single equation in ϕ, apply (23)–(25) to (7) to get

$$d^2\phi/dt^2 + B\phi + \frac{gc}{\phi^2} - af = 0, \quad B \equiv f^2 + 2gD_0/L^2. \tag{26}$$

In Appendix A we show how Thacker's (57) and (58) can be reduced to this equation.

Multiplying (26) by $d\phi/dt$ and integrating yields

$$(d\phi/dt)^2 + B\phi^2 - \frac{2gc}{\phi} - 2af\phi = e, \tag{27}$$

where e is another integration constant. The qualitative behaviour of ϕ and its exact solution in terms of elliptic integrals is examined in the next section. For now, we regard ϕ as known, and proceed to the integration of the remaining equations.

4.2. *Non-divergent flow*

Applying (23) and (25) to (11), leads to an expression for u_0 in terms of h_x and ϕ:

$$cu_0 = -\phi \frac{d}{dt}(\phi^2 h_x). \tag{28}$$

Applying (23) and (28) to (10) and rearranging leads to $(d/dt)[\phi^4 h_x^2 - 2c\phi(D_0 + h_0)] = 0$, or

$$\phi^4 h_x^2 - 2c\phi(D_0 + h_0) = b. \tag{29}$$

Applying (24) and (28) to (8) and rearranging leads to $(d/dt)[cv_0 - a\phi^2 h_x] = 0$, or

$$cv_0 = a\phi^2 h_x + d. \tag{30}$$

Here b and d are integration constants. Equations (28)–(30) express u_0, v_0 and h_0 in terms of ϕ and h_x (since $c \neq 0$). Applying (23), (28) and (30) to (6) results in a linear equation for h_x,

$$\frac{d^2 h_x}{dt^2} + \left(\frac{6}{\phi}\frac{d\phi}{dt}\right)\frac{dh_x}{dt} + h_x\left[\frac{6}{\phi^2}\left(\frac{d\phi}{dt}\right)^2 + \frac{2}{\phi}\frac{d^2\phi}{dt^2} - \frac{gc}{\phi^3} + \frac{fa}{\phi}\right] + \frac{fd}{\phi^3} = 0. \tag{31}$$

Equation (31) is freed of a first-derivative term by defining $H \equiv \phi^3 h_x$, so that

$$\frac{d^2 H}{dt^2} + H\left[\frac{fa}{\phi} - \frac{1}{\phi}\frac{d^2\phi}{dt^2} - \frac{gc}{\phi^3}\right] + fd = 0. \tag{32}$$

Fortuitously, the coefficient of H is equal to B (see (26)), and (32) reduces to

$$d^2 H/dt^2 + BH + fd = 0. \tag{33}$$

Solving (33), we obtain h_x as

$$h_x = \frac{1}{\phi^3}[\delta + \epsilon t - \tfrac{1}{2}fdt^2], \qquad\qquad B = 0,$$

$$h_x = \frac{1}{\phi^3}\left[\epsilon\sin(B^{1/2}t - \delta) - \frac{fd}{B}\right], \qquad\qquad B > 0, \left.\begin{matrix} \\ \\ \\ \\ \\ \\ \end{matrix}\right\} \tag{34}$$

$$h_x = \frac{1}{\phi^3}\left[\epsilon\exp((-B)^{1/2}t) + \delta\exp(-(-B)^{1/2}t) - \frac{fd}{B}\right], \quad B < 0,$$

where ϵ and δ are constants. These solutions correspond to the non-divergent solutions of the previous section, (20)–(22), modulated by the divergent mode (the factor of ϕ^3).

4.3. *Shoreline*

The shoreline is defined by the points $x = r$ for which $D(r) + h(r, t) = 0$, or, in view of (4),

$$D_0(1 - r^2/L^2) + h_0 + h_x r + \tfrac{1}{2}h_{xx} r^2 = 0. \tag{35}$$

Solving (35) for r yields

$$r = -\left(\frac{h_x}{h_{xx} - 2D_0/L^2}\right) \pm \left[\left(\frac{h_x}{h_{xx} - 2D_0/L^2}\right)^2 - 2\left(\frac{h_0 + D_0}{h_{xx} - 2D_0/L^2}\right)\right]^{1/2}, \tag{36}$$

from which one can infer that the shoreline extends further up the sides of the channel as the free-surface curvature becomes more concave (or less convex).

Making use of (25) and (29), we rewrite (36) as

$$r_+ = -\frac{h_x\phi^3}{c} + b^{1/2}\left|\frac{\phi}{c}\right|, \quad r_- = -\frac{h_x\phi^3}{c} - b^{1/2}\left|\frac{\phi}{c}\right|, \tag{37}$$

where r_+ and r_- denote the positions of the eastern and western shorelines, respectively. The $\phi^3 h_x$ terms in this expression are known explicitly from (34).

5. Solution of the ϕ-equation

We non-dimensionalize (27) by introducing $\tau \equiv |B|^{1/2} t$ (for $B \neq 0$), $\alpha^3 \equiv -2gc/|B|$, $\Phi \equiv \phi/\alpha$, $A \equiv -2af/(\alpha|B|)$ and $E \equiv e/(\alpha^2|B|)$, obtaining

$$(d\Phi/d\tau)^2 \pm \Phi^2 + 1/\Phi + A\Phi = E, \tag{38}$$

where the upper sign is taken if $B > 0$ and the lower sign is taken if $B < 0$.

In view of (25) and the parameters introduced above we can write

$$\Phi = -\left[\frac{|B|}{2g(h_{xx} - 2D_0/L^2)}\right]^{1/3}. \tag{39}$$

For the main case of interest, $h_{xx} - 2D_0/L^2 < 0$ (see §2), and Φ is positive.

In view of (24), (25) and the parameters introduced above, we can express A as

$$A = \left(\frac{4}{g|B|^2}\right)^{1/3} \frac{f(v_x + f)}{(h_{xx} - 2D_0/L^2)^{1/3}}. \tag{40}$$

With $h_{xx} - 2D_0/L^2 < 0$, A is positive if $f(v_x + f) < 0$ and negative if $f(v_x + f) > 0$.

To solve our problem with specified initial values of $h_{xx}(0)$, $v_x(0)$ and $u_x(0)$, we compute A from (40), $\Phi(0)$ from (39) and $(d\Phi/d\tau)(0)$ from (23), that is $(d\Phi/d\tau)$ $(0) = \Phi(0)u_x(0)|B|^{-1/2}$. We then obtain E as a residual from (38) and solve (38) with the initial value $\Phi(0)$.

The qualitative behaviour of Φ can be deduced by analogy to one-dimensional particle motion in a potential field, that is by regarding Φ as a particle displacement and (38) as an energy equation for a conservative system (Goldstein 1980). In §5.1 we describe the qualitative behaviour of the solution under the restriction that $B > 0$. The corresponding exact solution is presented in §5.2. Exact solutions for $B < 0$ and $B = 0$ are presented in §§5.3 and 5.4.

5.1. *Qualitative behaviour of the solution for $B > 0$*

If $B > 0$ then (38) can be written as

$$(d\Phi/d\tau)^2 + V(\Phi) = E, \quad V(\Phi) \equiv \Phi^2 + 1/\Phi + A\Phi, \tag{41}$$

where we regard $(d\Phi/d\tau)^2$ as the kinetic energy and $V(\Phi)$ as a nonlinear potential energy function. Since $(d\Phi/d\tau)^2$ is non-negative, $V(\Phi)$ must be less than or equal to E on any domain of physical interest. The behaviour of the solution depends on the nature of $V(\Phi)$, especially on the points Φ^* where $V(\Phi^*) = E$. Since $d\Phi/d\tau = 0$ on these points, Φ^* are local extrema of $\Phi(t)$. As long as $\Phi^* \neq 0$, these points are equivalent to the roots of $\Phi^*[V(\Phi^*) - E] = 0$, that is the roots of the cubic equation $\Phi^{*3} + A\Phi^{*2} - E\Phi^* + 1 = 0$. These roots are derived in Appendix B.

Since $dV/d\Phi = 2\Phi - 1/\Phi^2 + A$, there are local extrema in $V(\Phi)$ where $\Phi^3 + \frac{1}{2}A\Phi^2 - \frac{1}{2} = 0$. Analysis of this cubic equation following the general procedure in Appendix B reveals that there are one, two or three extrema depending on whether A is less than, equal to, or greater than 3.

$V(\Phi)$ is split into two curves by the singularity at $\Phi = 0$. On the curve for $\Phi > 0$, the curvature is always positive, $\lim_{\Phi \to \infty} V(\Phi) = \infty$ and $\lim_{\Phi \to 0} V(\Phi) = \infty$. Thus, there is only one extremum for $\Phi > 0$ and it is a minimum. On the curve for $\Phi < 0$, V has positive curvature for $\Phi < -1$, negative curvature for $\Phi \in (-1, 0)$, and an inflection point at $\Phi = -1$. Moreover, $\lim_{\Phi \to 0} V(\Phi) = -\infty$ and $\lim_{\Phi \to -\infty} V(\Phi) = \infty$. If $A < 3$ there are no local extrema for $\Phi < 0$ since there is only one local extremum on the
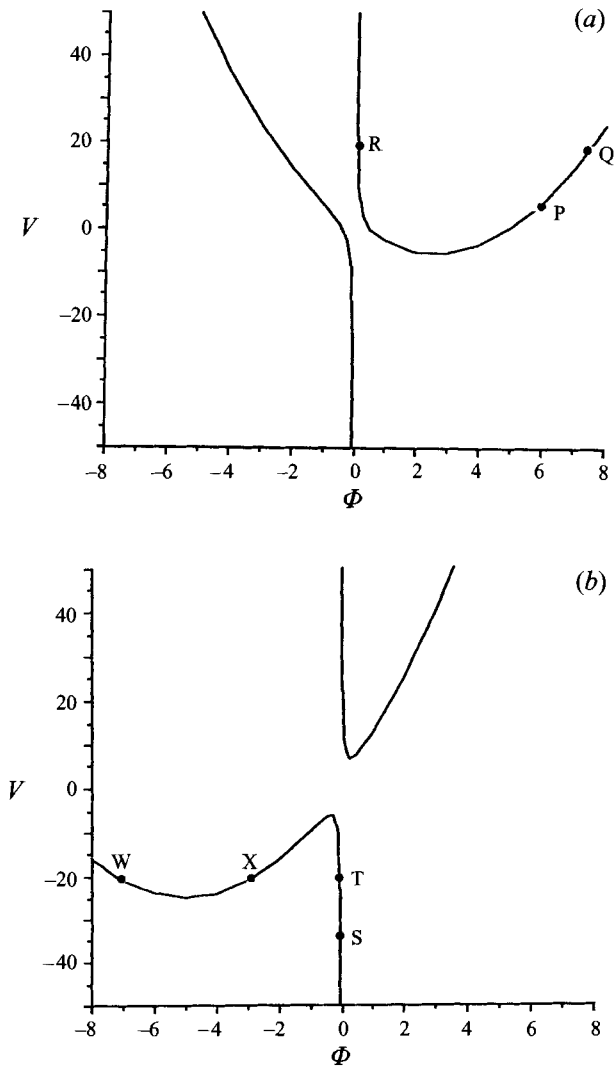
FIGURE 2. Representative curves of the potential energy function $V(\Phi) \equiv \Phi^2 + 1/\Phi + A\Phi$ for $B > 0$. (a) $A = -5$, (b) $A = 10$. Points R and Q in (a) mark the turning points of the solution for $E = 20$. Points W and X in (b) mark the turning points of the solution for $E = -20$.

whole domain $\Phi \in (-\infty, \infty)$ and it is associated with the curve for $\Phi > 0$. If $A > 3$ there are two local extrema for $\Phi < 0$: a local minimum for $\Phi \in (-\infty, -1)$, and a local maximum for $\Phi \in (-1, 0)$. $V(\Phi)$ curves representative of the regimes where A is less than 3 (one local extremum) and greater than 3 (three local extrema) are depicted in figure 2.

To illustrate the qualitative behaviour of Φ, let the initial values $h_{xx}(0)$, $v_x(0)$ and $u_x(0)$ be such that $A = -5$, $E = 20$ and $\Phi(0) = 6$ (point P on figure 2a). The subsequent motion must satisfy (41), which we write as

$$d\Phi/d\tau = \pm [E - V(\Phi)]^{1/2}. \tag{42}$$

If we choose the positive branch of (42) the motion proceeds along the $V(\Phi)$ curve in the direction of increasing Φ until a point where $V(\Phi) = E$ is reached (point Q).

Although $\mathrm{d}\Phi/\mathrm{d}\tau = 0$ at Q, the solution will, in general, not be in a steady state because $\mathrm{d}^2\Phi/\mathrm{d}\tau^2$ is not necessarily zero ($\mathrm{d}^2\Phi/\mathrm{d}\tau^2$ vanishes only where $\mathrm{d}V/\mathrm{d}\Phi$ vanishes). Moreover, the solution cannot proceed further in the direction of increasing Φ because $E - V(\Phi)$ would then be negative. Therefore, we must now choose the negative branch of (42), and proceed along the $V(\Phi)$ curve in the direction of decreasing Φ until the next root of $V(\Phi) - E = 0$ is reached (point R). $\mathrm{d}\Phi/\mathrm{d}\tau$ changes sign at this point and Φ subsequently increases. This process continues *ad infinitum* and we infer an oscillatory motion between points Q and R. This oscillatory motion would have been identical, apart from a phase shift, if we have started at any point between Q and R with either the negative or positive branch of (42).

Now suppose that $A = 10$, $E = -20$ and the initial value $\Phi(0)$ is negative (the fluid depth becomes infinite as $x \to \pm\infty$). This initial state is point S in figure 2(*b*). If the motion starts along the positive branch of (42) it continues along the positive branch for all time since it never reaches a turning point. As $t \to \infty$, $\Phi \to 0$ and the potential and kinetic energies become unbounded. If the motion starts at S along the negative branch of (42), a turning point is eventually reached (point T) and the solution thereafter proceeds along the positive branch. Again, the potential and kinetic energies become unbounded. If the motion starts at any point between the two turning points W and X, an oscillatory motion would result.

5.2. *Exact solution for $B > 0$*

Separating variables in (42) and integrating, we obtain

$$\tau = \mathrm{const} \pm \int^{\Phi} \left[\frac{\Phi'}{E\Phi' - A\Phi'^2 - 1 - \Phi'^3} \right]^{1/2} \mathrm{d}\Phi'. \tag{43}$$

Restricting attention to the oscillatory motion associated with $\Phi > 0$, the denominator of (43) has three real roots, Φ_1^*, Φ_2^* and Φ_3^*; two positive and one negative. Here we order these roots (and rename them) as Φ_1, Φ_2 and Φ_3 where $\Phi_3 > \Phi_2 > 0 > \Phi_1$. The motion is such that Φ oscillates between the two positive roots Φ_2 and Φ_3. It is convenient to start the motion at $\Phi(0) = \Phi_2$ (so $u_x(0) = 0$, and $v_x(0)$ and $h_{xx}(0)$ are local extrema). The solution must then proceed along the positive branch of (43) and satisfy

$$\tau = \tau(\Phi_2, \Phi) \equiv \int_{\Phi_2}^{\Phi} \left[\frac{\Phi'}{(\Phi' - \Phi_1)(\Phi' - \Phi_2)(\Phi_3 - \Phi')} \right]^{1/2} \mathrm{d}\Phi', \tag{44}$$

where $\Phi_3 \geqslant \Phi > \Phi_2 > 0 > \Phi_1$. The solution reaches the turning point $\Phi = \Phi_3$ at $\tau = \tau(\Phi_2, \Phi_3)$ and then proceeds along the negative branch of (43). Thus, for the second half of this oscillation,

$$\tau = \tau(\Phi_2, \Phi_3) - \int_{\Phi_3}^{\Phi} \left[\frac{\Phi'}{(\Phi' - \Phi_1)(\Phi' - \Phi_2)(\Phi_3 - \Phi')} \right]^{1/2} \mathrm{d}\Phi' = 2\tau(\Phi_2, \Phi_3) - \tau(\Phi_2, \Phi). \tag{45}$$

The solution completes one period of oscillation T_{23} ($\equiv 2\tau(\Phi_2, \Phi_3)$) when Φ returns to Φ_2.

The integral $\tau(\Phi_2, \Phi)$ is evaluated with the aid of Gradshteyn & Ryzhik (1980, equation (14) of §3.167). Collecting results, we write the solution over a period T_{23} of this oscillation as

$$\tau = \tau(\Phi_2, \Phi) = \frac{2\Phi_2}{[\Phi_3(\Phi_2 - \Phi_1)]^{1/2}} \Pi\left(\chi, 1 - \frac{\Phi_2}{\Phi_3}, \rho \right), \tag{46}$$

as Φ travels from Φ_2 to Φ_3 $(0 < \tau \leqslant T_{23}/2)$, and

$$\tau = T_{23} - \tau(\Phi_2, \Phi), \tag{47}$$

as Φ travels from Φ_3 back to Φ_2 $(\frac{1}{2}T_{23} < \tau < T_{23})$, where

$$T_{23} = \frac{4\Phi_2}{[\Phi_3(\Phi_2 - \Phi_1)]^{1/2}} \Pi\left(\frac{\pi}{2}, 1 - \frac{\Phi_2}{\Phi_3}, \rho\right), \tag{48}$$

$$\chi \equiv \arcsin\left[\frac{\Phi_3}{\Phi}\frac{(\Phi - \Phi_2)}{(\Phi_3 - \Phi_2)}\right]^{1/2}, \quad \rho \equiv \left[-\frac{\Phi_1}{\Phi_3}\frac{(\Phi_3 - \Phi_2)}{(\Phi_2 - \Phi_1)}\right]^{1/2},$$

and $\Pi(\chi, 1 - \Phi_2/\Phi_3, \rho)$ is a Legendre elliptic integral of the third kind (notation as in Gradshteyn & Ryzhik). If the motion starts at $\Phi(0) = \Phi_3$ rather than at Φ_2, a simple modification of this solution is required (with no change in T_{23}).

5.3. *Exact solution for $B < 0$*

If $B < 0$, equation (38) becomes

$$\left(\frac{d\Phi}{d\tau}\right)^2 + V(\Phi) = E, \quad V(\Phi) \equiv -\Phi^2 + \frac{1}{\Phi} + A\Phi. \tag{49}$$

The $V(\Phi)$ curve for $B < 0$ is identical to the curve for $B > 0$ with V replaced by $-V$ and Φ replaced by $-\Phi$, that is the curve $V(\Phi)$ for $B < 0$ can be obtained by reflecting the curve $V(\Phi)$ for $B > 0$ about the Φ- and V-axes. Similarly, the roots Φ^* of $E - V(\Phi^*) = 0$ for $B < 0$ are equal to the negative of the roots of $E - V(\Phi^*) = 0$ for $B > 0$ with E replaced by $-E$.

For $B < 0$, the only scenario of oscillatory motion is when all three roots of $E - V = 0$ are real and positive, and the flow is confined to the basin between the first and second roots Φ_1 and Φ_2 (with the roots ordered as $0 < \Phi_1 < \Phi_2 < \Phi_3$). As in the previous section, we start the motion at a root of $E - V = 0$, in this case $\Phi(0) = \Phi_1$, so u_x is initially zero and v_x and h_{xx} are local extrema. Making use of Gradshteyn & Ryzhik (1980, integral (4) of §3.167), we write the solution over a period T_{12} of this oscillation as

$$\tau = \tau(\Phi_1, \Phi) \equiv \frac{2\Phi_1}{[\Phi_2(\Phi_3 - \Phi_1)]^{1/2}} \Pi\left(X, 1 - \frac{\Phi_1}{\Phi_2}, P\right), \tag{50}$$

as Φ travels from Φ_1 to Φ_2 $(0 < \tau \leqslant \frac{1}{2}T_{12})$, and

$$\tau = T_{12} - \tau(\Phi_1, \Phi), \tag{51}$$

as Φ travels from Φ_2 back to Φ_1 $(\frac{1}{2}T_{12} < \tau < T_{12})$, where

$$T_{12} = \frac{4\Phi_1}{[\Phi_2(\Phi_3 - \Phi_1)]^{1/2}} \Pi\left(\frac{1}{2}\pi, 1 - \frac{\Phi_1}{\Phi_2}, P\right), \tag{52}$$

$$X \equiv \arcsin\left[\frac{\Phi_2}{\Phi}\frac{(\Phi - \Phi_1)}{(\Phi_2 - \Phi_1)}\right]^{1/2}, \quad P \equiv \left[\frac{\Phi_3}{\Phi_2}\frac{(\Phi_2 - \Phi_1)}{(\Phi_3 - \Phi_1)}\right]^{1/2}.$$

If the motion starts at $\Phi(0) = \Phi_2$ rather than at Φ_1, a simple modification of this solution is required.

5.4. *Exact solution for $B = 0$*

If $B = 0$, we introduce $\alpha \equiv -2gc$, $\Phi \equiv \phi/\alpha$, $\tau \equiv t/\alpha$ and $\kappa \equiv 4afgc$, and (27) becomes

$$d\Phi/d\tau = \pm[e - V(\Phi)]^{1/2}, \quad V(\Phi) = 1/\Phi + \kappa\Phi. \tag{53}$$

Again, because of the singularity at $\Phi = 0$, $V(\Phi)$ is composed of two curves, one for $\Phi > 0$ and one for $\Phi < 0$. Since $dV/d\Phi = -1/\Phi^2 + \kappa$ and $d^2V/d\Phi^2 = 2/\Phi^3$, we see that if $\kappa > 0$ there is a local minimum $V_{min} = 2\kappa^{1/2}$ at $\Phi = \kappa^{-1/2}$ and a local maximum $V_{max} = -2\kappa^{1/2}$ at $\Phi = -\kappa^{-1/2}$. If $\kappa < 0$ then $dV/d\Phi < 0$ everywhere. If $\kappa = 0$ then $dV/d\Phi < 0$ but approaches 0 as $\Phi \to \pm\infty$. Thus, if $\kappa > 0$ and $\Phi > 0$ there is an oscillation in the $V(\Phi)$ basin provided that $e > V_{min}$. If $\kappa = 0$ and $\Phi > 0$ then $\Phi \to \infty$ as $t \to \infty$ (so $d\Phi/d\tau \to e^{1/2}$ and $u_x \to 0$ as $t \to \infty$) either directly or after going through a turning point at $\Phi = 1/e$. If $\kappa < 0$ the kinetic energy becomes unbounded on either curve.

First consider the oscillatory motion associated with $\kappa > 0$. The two turning points are given by

$$\Phi_1 = \frac{e}{2\kappa}\left[1 - \left(1 - \frac{4\kappa}{e^2}\right)^{1/2}\right], \quad \Phi_2 = \frac{e}{2\kappa}\left[1 + \left(1 - \frac{4\kappa}{e^2}\right)^{1/2}\right]. \tag{54}$$

The condition for oscillatory motion, $e > V_{min} = 2\kappa^{1/2}$, guarantees that these turning points are real and positive. We start the motion at $\tau = 0$ at Φ_1 and proceed in the direction of increasing Φ (the positive branch of (53)). Thus, for the first half of this oscillation we have

$$\tau = \tau(\Phi_1, \Phi) \equiv \frac{1}{\kappa^{1/2}}\int_{\Phi_1}^{\Phi}\left[\frac{\Phi'}{(\Phi' - \Phi_1)(\Phi_2 - \Phi')}\right]^{1/2}d\Phi', \tag{55}$$

where $\Phi_1 < \Phi_2$. The solution reaches the second turning point when $\tau = \tau(\Phi_1, \Phi_2)$. For the second half of the oscillation the solution follows the negative branch of (53) so that

$$\tau = \tau(\Phi_1, \Phi_2) - \frac{1}{\kappa^{1/2}}\int_{\Phi_2}^{\Phi}\left[\frac{\Phi'}{(\Phi' - \Phi_1)(\Phi_2 - \Phi')}\right]^{1/2}d\Phi' = 2\tau(\Phi_1, \Phi_2) - \tau(\Phi_1, \Phi). \tag{56}$$

The solution completes one period of oscillation $T_{12}(\equiv 2\tau(\Phi_1, \Phi_2))$ when Φ returns to Φ_1.

The integral $\tau(\Phi_1, \Phi)$ is evaluated with the aid of Gradshteyn & Ryzhik (1980, equation (16) of §3.141). Collecting results, we write the solution over one period T_{12} as

$$\tau = \tau(\Phi_1, \Phi) = 2\left(\frac{\Phi_2}{\kappa}\right)^{1/2}E(\chi, P) - 2\left[\frac{(\Phi - \Phi_1)(\Phi_2 - \Phi)}{\kappa\Phi}\right]^{1/2}, \tag{57}$$

as Φ travels from Φ_1 to Φ_2 $(0 < \tau \leqslant \frac{1}{2}T_{12})$, and

$$\tau = T_{12} - \tau(\Phi_1, \Phi), \tag{58}$$

as Φ travels from Φ_2 back to Φ_1 $(\frac{1}{2}T_{12} < \tau < T_{12})$, where

$$T_{12} = 4(\Phi_2/\kappa)^{1/2}E(\tfrac{1}{2}\pi, P), \tag{59}$$

$$\chi \equiv \arcsin\left[\frac{\Phi_2(\Phi - \Phi_1)}{\Phi(\Phi_2 - \Phi_1)}\right]^{1/2}, \quad P \equiv \left(1 - \frac{\Phi_1}{\Phi_2}\right)^{1/2},$$

and $E(\chi, P)$ is a Legendre elliptic integral of the second kind.

Next consider the case where $\kappa = 0$. Since $B(\equiv f^2 + 2gD_0/L^2)$ is also 0, this corresponds to either (i) the spreading of a non-rotating parabolic ridge of fluid over a flat plane or (ii) the spreading of a rotating parabolic ridge of fluid over a parabolic ridge with $D_0 = -f^2L^2/(2g)$. The spreading of a rotating parabolic ridge of fluid over

a flat plane is contained in the $B > 0$ flows described in §§5.1 and 5.2. The related case of axisymmetric spreading of a paraboloid of revolution was considered by Ball (1964) and Thacker (1981).

If the motion starts at the unique turning point $\Phi = 1/e(> 0)$, the solution satisfies

$$\tau = \int_{1/e}^{\Phi} \left(\frac{\Phi'}{e\Phi' - 1} \right)^{1/2} d\Phi'. \tag{60}$$

Evaluation of the integral is facilitated by changing variables to $x = [e\Phi'/(e\Phi' - 1)]^{1/2}$. One obtains

$$\tau = \frac{1}{e^{3/2}} \left[[e\Phi(e\Phi - 1)]^{1/2} - \tfrac{1}{2} \ln \left(\frac{(e\Phi)^{1/2} - (e\Phi - 1)^{1/2}}{(e\Phi)^{1/2} + (e\Phi - 1)^{1/2}} \right) \right]. \tag{61}$$

6. Recapitulation: the initial value problem

The solutions of the Φ-equation described in §5 were constructed so that the initial values $\Phi(0)$ were associated with a zero in $d\Phi/d\tau$ (i.e. $u_x(0) = 0$, and $v_x(0)$ and $h_{xx}(0)$ are local extrema); this choice simplified the form of the solutions without limiting their generality (apart from the removal of a phase shift). The form of these solutions depended on the sign of B. We now summarize the solution for all variables for $B > 0$ and indicate how the constants of integration can be related to the initial conditions and the governing parameters. The channel geometry and Coriolis parameter are assumed specified at the outset.

Specified initial values of the free-surface curvature $h_{xx}(0)$ and relative vorticity $v_x(0)$ allow us to compute A from (40) and $\Phi(0)$ from (39). Thus, with A and $\Phi(0)$ known and $d\Phi/d\tau(0) = 0$, we compute E as a residual from (38). The three roots $\Phi_1 < \Phi_2 < \Phi_3$ are obtained by ordering the roots in (B 5). If $h_{xx}(0) - 2D_0/L^2 < 0$ then $\Phi_1 < 0 < \Phi_2 < \Phi_3$ and $\Phi(0)$ is equal to one of the positive roots, Φ_2 or Φ_3. If $\Phi(0) = \Phi_2$, the solution for Φ (an oscillation between Φ_2 and Φ_3) follows from (46)–(48). If $\Phi(0) = \Phi_3$ then Φ follows from a simple modification of (46)–(48). The solution for $d\Phi/d\tau$ in terms of Φ follows from (42). We obtain u_x, v_x and h_{xx} from (23), (24) and (25) rewritten as

$$u_x = \frac{1}{\phi} \frac{d\phi}{dt} = \frac{|B|^{1/2}}{\Phi} \frac{d\Phi}{d\tau}, \tag{62}$$

$$v_x + f = \frac{\tilde{a}}{\Phi}, \quad \text{where} \quad \tilde{a} \equiv \frac{a}{\alpha} = -\frac{A|B|}{2f}, \tag{63}$$

$$h_{xx} - \frac{2D_0}{L^2} = \frac{\tilde{c}}{\Phi^3}, \quad \text{where} \quad \tilde{c} \equiv \frac{c}{\alpha^3} = -\frac{|B|}{2g}, \tag{64}$$

and h_x, v_0 and u_0 follow from (34), (30) and (28) as

$$h_x = \frac{1}{\Phi^3} \left[\tilde{\epsilon} \sin(\tau - \delta) - \frac{f\tilde{d}}{B} \right], \quad \tilde{d} \equiv \frac{d}{\alpha^3}, \quad \tilde{\epsilon} \equiv \frac{\epsilon}{\alpha^3}, \tag{65}$$

$$v_0 = \frac{\tilde{a}}{\tilde{c}\Phi} \left[\tilde{\epsilon} \sin(\tau - \delta) - \frac{f\tilde{d}}{B} \right] + \frac{\tilde{d}}{\tilde{c}}, \tag{66}$$

$$u_0 = -\frac{|B|^{1/2}\tilde{\epsilon}}{\tilde{c}} \cos(\tau - \delta) + \frac{|B|^{1/2}}{\tilde{c}\Phi} \frac{d\Phi}{d\tau} \left[\tilde{\epsilon} \sin(\tau - \delta) - \frac{f\tilde{d}}{B} \right]. \tag{67}$$

The constants $\tilde{d}, \delta$ and $\tilde{\epsilon}$ are related to the initial values $h_x(0)$, $v_0(0)$ and $u_0(0)$ by

$$\tilde{d} = \tilde{c} v_0(0) - \tilde{a} \Phi^2(0) h_x(0), \tag{68}$$

$$\delta = \arctan\left[\frac{|B|^{1/2}}{\tilde{c} u_0(0)}\left(\Phi^3(0) h_x(0) + \frac{f\tilde{d}}{B}\right)\right], \tag{69}$$

$$\tilde{\epsilon} = -\frac{\tilde{c} u_0(0)}{|B|^{1/2} \cos \delta}, \quad \cos \delta \neq 0,$$

$$= -\frac{\Phi^3(0) h_x(0) + f\tilde{d}/B}{\sin \delta}, \quad \sin \delta \neq 0. \tag{70}$$

We obtain h_0 from (29) rewritten as

$$h_0 = \frac{\Phi^3 h_x^2}{2\tilde{c}} - \frac{\tilde{b}}{2\tilde{c}\Phi} - D_0, \quad \tilde{b} = \frac{b}{\alpha^4}. \tag{71}$$

The parameter b (or $\tilde{b}$) affects the fluid depth at the centreline $D_0 + h_0$ and the shoreline positions r_+ and r_-, but does not affect $u_0, v_0, h_x, v_x, h_{xx}$ or u_x. If $D_0 > 0$ we choose b such that the total fluid mass (per unit y-length) in the channel is equal to the mass in an undisturbed channel with a planar free-surface at $z = 0$, that is

$$\int_{r_-(t)}^{r_+(t)} (D(x) + h(x, t))\, \mathrm{d}x = \int_{-L}^{L} D(x)\, \mathrm{d}x. \tag{72}$$

Using (4), (29), (37) and the condition $h_{xx} - 2D_0/L^2 < 0$ to evaluate (72), we obtain b as

$$b = (2D_0 L c^2)^{2/3}, \quad \tilde{b} = b/\alpha^4 = (2D_0 L \tilde{c}^2)^{2/3} = (D_0 L B^2/2g^2)^{2/3}. \tag{73}$$

If the flow takes place over a ridge ($D_0 < 0$) or over a flat plane ($D_0 = 0$) it may be more appropriate to specify an arbitrary initial centreline depth and compute b from (71) as a residual.

The shoreline functions are obtained from (37) rewritten as

$$r_+ = -\frac{\tilde{\epsilon}}{\tilde{c}} \sin(\tau - \delta) + \frac{f\tilde{d}}{B\tilde{c}} + \tilde{b}^{1/2}\left|\frac{\Phi}{\tilde{c}}\right|, \quad r_- = -\frac{\tilde{\epsilon}}{\tilde{c}} \sin(\tau - \delta) + \frac{f\tilde{d}}{B\tilde{c}} - \tilde{b}^{1/2}\left|\frac{\Phi}{\tilde{c}}\right|. \tag{74}$$

7. Trajectories

The class of flows considered herein are noteworthy in that flow trajectories can be obtained analytically. The trajectories are solutions of (5) with $x(t)$ and $y(t)$ regarded as the instantaneous position coordinates of a fluid parcel. Since $u = \mathrm{d}x/\mathrm{d}t$ and $v = \mathrm{d}y/\mathrm{d}t$, (5) becomes

$$\mathrm{d}x/\mathrm{d}t = u_0(t) + u_x(t) x(t), \quad \mathrm{d}y/\mathrm{d}t = v_0(t) + v_x(t) x(t). \tag{75}$$

We solve these equations for the case where $B > 0$ and $h_{xx} - 2D_0/L^2 < 0$. Ironically, the evaluation of the y-component of the trajectory for these 'one-dimensional' flows offers the most difficulty.

7.1. *x-component of the trajectory*

Making use of (23), we can integrate the first of (75) as

$$x(t) = x(0)\frac{\Phi(t)}{\Phi(0)} + \Phi(t) \int_0^t \frac{u_0(t')}{\Phi(t')}\, \mathrm{d}t'. \tag{76}$$

The integral is evaluated with the aid of (28) and (34) and we obtain

$$x(t) = \frac{\Phi(t)}{\Phi(0)}\left(x(0) + \frac{\Phi^3(0)\,h_x(0)}{\tilde{c}}\right) - \frac{\tilde{\epsilon}}{\tilde{c}}\sin\left(B^{1/2}\,t - \delta\right) + \frac{f\tilde{d}}{B\tilde{c}}. \tag{77}$$

7.2. y-component of the trajectory

Making use of (24), (30), (34) and (77), the y-component trajectory equation becomes

$$\frac{\mathrm{d}y}{\mathrm{d}t} = v_0(0) + \tilde{a}\frac{x(0)}{\Phi(0)} - fx(t), \tag{78}$$

which integrates to

$$y = y(0) + \left(v_0(0) + \tilde{a}\frac{x(0)}{\Phi(0)}\right)t - f\int_0^t x(t')\,\mathrm{d}t'. \tag{79}$$

If $f = 0$ then (79) is our desired formula. If $f \neq 0$, apply (77) in (79) so that

$$y = y(0) + \left(v_0(0) + \tilde{a}\frac{x(0)}{\Phi(0)}\right)t + \frac{f}{\tilde{c}}\int_0^t \Phi^3(t')\,h_x(t')\,\mathrm{d}t'$$

$$- \frac{f}{\tilde{c}\Phi(0)}\left(\tilde{c}x(0) + \Phi^3(0)\,h_x(0)\right)\int_0^t \Phi(t')\,\mathrm{d}t'. \tag{80}$$

The $\Phi^3 h_x$ integral can be easily evaluated with the aid of (34). The integral over Φ is more difficult since we only know Φ implicitly. In this case we change the integration variable from t to Φ,

$$I \equiv \int_0^t \Phi(t')\,\mathrm{d}t' = \int_{\Phi(0)}^{\Phi(t)} \frac{\Phi'}{\mathrm{d}\Phi'/\mathrm{d}t'}\,\mathrm{d}\Phi' = \frac{1}{|B|^{1/2}}\int_{\Phi(0)}^{\Phi(\tau)} \frac{\Phi'}{\mathrm{d}\Phi'/\mathrm{d}\tau'}\,\mathrm{d}\Phi'. \tag{81}$$

In practice this integral must be partitioned into subintervals such that $\mathrm{d}\Phi'/\mathrm{d}\tau$ vanishes at the endpoints of each subinterval.

In the case where $B > 0$ and $h_{xx} - 2D_0/L^2 < 0$, Φ oscillates between the two turning points Φ_2 and Φ_3 with a (non-dimensional) period T_{23} (see §5.2). We start the motion at $\Phi(0) = \Phi_2$ and proceed along the positive branch of (42) until Φ_3 is reached. For the second half of the oscillation the motion proceeds along the negative branch of (42). Thus, for $0 < \tau \leqslant \frac{1}{2}T_{23}$ (the first half of the oscillation), the integral can be written as

$$I = I(\Phi_2, \Phi) \equiv \frac{1}{B^{1/2}}\int_{\Phi_2}^{\Phi} \frac{\Phi'^{3/2}}{[(\Phi' - \Phi_1)(\Phi' - \Phi_2)(\Phi_3 - \Phi')]^{1/2}}\,\mathrm{d}\Phi', \tag{82}$$

and for $T_{23}/2 < \tau < T_{23}$ (the second half of the oscillation), the integral becomes

$$I = 2I(\Phi_2, \Phi_3) - I(\Phi_2, \Phi). \tag{83}$$

The integral $I(\Phi_2, \Phi)$ is evaluated in Appendix C. Collecting results, we write the solution as

$$y = y(0) + \left(v_0(0) + \tilde{a}\frac{x(0)}{\Phi(0)}\right)t + \frac{f\tilde{\epsilon}}{\tilde{c}B^{1/2}}[\cos\delta - \cos(B^{1/2}\,t - \delta)] - \frac{f^2\tilde{d}}{\tilde{c}B}t$$

$$- \frac{f}{\tilde{c}\Phi(0)}\left(\tilde{c}x(0) + \Phi^3(0)\,h_x(0)\right) \times \begin{cases} I(\Phi_2, \Phi) & \text{for} \quad 0 < \tau \leqslant \frac{1}{2}T_{23}, \\ 2I(\Phi_2, \Phi_3) - I(\Phi_2, \Phi) & \text{for} \quad \frac{1}{2}T_{23} < \tau < T_{23}, \end{cases} \tag{84}$$

where $I(\Phi_2, \Phi)$ is given by (C 8). The extension of this solution for non-dimensional

times greater than T_{23} and for a motion that starts at $\Phi(0) = \Phi_3$ rather than at Φ_2 is straightforward.

7.3. *z-component of the trajectory*

For the vertical component of the trajectory we use the familiar result in shallow-water theory that the relative height of a fluid element above the lower boundary is conserved following the motion of the fluid element (Pedlosky 1979). For a flow satisfying (4) and (5), this can be expressed as

$$z(t) = -D(x(t)) + \left(\frac{D(x(t)) + h_0(t) + x(t)h_x(t) + \frac{1}{2}x^2(t)h_{xx}(t)}{D(x(0)) + h_0(0) + x(0)h_x(0) + \frac{1}{2}x^2(0)h_{xx}(0)} \right) [z(0) + D(x(0))]. \quad (85)$$

8. Examples

In order to quantitatively evaluate the solution and trajectories for specific flow scenarios, it was necessary to evaluate the Legendre elliptic integrals of the first, second and third kind. Toward that end, we computed the Carlson elliptic integrals with the IMSL MATH/LIBARARY special functions FORTRAN subroutines ELRF, ELRD and ELRJ. The Legendre elliptic integrals were then expressed in terms of the Carlson integrals following the relations given in Carlson (1979, p. 8) (see also Press *et al.* 1992, §6.11).

We first examine the behaviour of the non-dimensional period of oscillation T_{23} for the divergent mode described in §5.2. We will display T_{23} as a function of two non-dimensional parameters:

$$\mu_1 \equiv \frac{g(h_{xx}^* - 2D_0/L^2)}{B} = \frac{gh_{xx}^*/f^2 - 2L_R^2/L^2}{1 + 2L_R^2/L^2} \quad (86)$$

and

$$\mu_2 \equiv \frac{f(v_x^* + f)}{B} = \frac{1 + v_x^*/f}{1 + 2L_R^2/L^2}. \quad (87)$$

Here $L_R \equiv (gD_0)^{1/2}/|f|$ is the Rossby radius of deformation and v_x^* and h_{xx}^* are extrema in the relative vorticity and free-surface curvature, respectively. A and the extremum $\Phi(0)$ are related to μ_1 and μ_2 through (39) and (40), i.e. $A = 4^{1/3}\mu_2\mu_1^{-1/3}$ and $\Phi(0) = -(2\mu_1)^{-1/3}$. A contour plot of T_{23} as a function of μ_1 and μ_2 is presented in figure 3. The period of oscillation is seen to increase as μ_1 decreases and as μ_2 increases. It can be shown that if $f \rightarrow \pm \infty$ (with other parameters held fixed) then $\mu_1 \rightarrow 0$, $\mu_2 \rightarrow 1$, $\Phi \rightarrow \infty$ and $T_{23} \rightarrow 4\Pi(\frac{1}{2}\pi, 0, 0) = 2\pi$. In this case the amplitude of the divergent oscillation vanishes while the dimensional period of the oscillation, $2\pi/B^{1/2}$, becomes equal to the period of the non-divergent mode (see §3).

We next examine the velocity and free-surface displacement functions for a flow in which the free surface is initially a parabolic ridge centred on the channel centreline. We consider three scenarios: (i) $L > L_R$, (ii) $L \sim L_R$, and (iii) $L < L_R$. In all three cases the initial conditions are: $u_0(0) = 1$ m s^{-1}, $v_0(0) = 3$ m s^{-1}, $u_x(0) = 0$, $v_x(0) = 6/L$, $h_x(0) = 0$ and $h_{xx}(0) = -20D_0/L^2$. The channel depth is $D_0 = 10^3$ m, the (reduced) gravity constant is $g = 0.01 \times 9.8$ m s^{-2} and the Coriolis parameter is $f = 10^{-4}$ s^{-1}, giving a Rossby radius of deformation of $L_R \approx 10^5$ m. The channel half-width in case (i) is $L = 10^6$ m, in case (ii) is $L = 10^5$ m, and in case (iii) is $L = 10^4$ m. Some derived parameter values for these cases are presented in table 1. Time series for the divergent mode functions in cases (i), (ii) and (iii) are shown in figures 4, 6 and 8, respectively, for two periods of the divergent oscillation. Time series for the corresponding non-divergent flow variables in cases (i), (ii) and (iii) are shown in figures 5, 7 and 9,
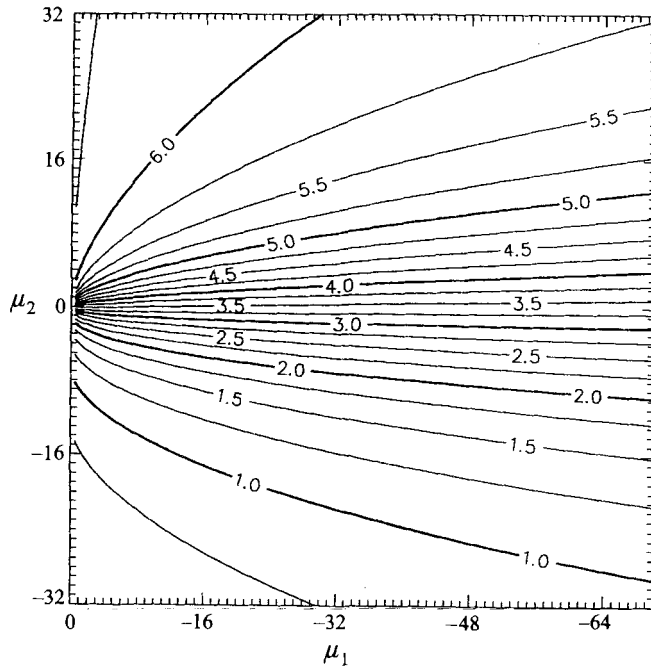
FIGURE 3. Non-dimensional period of oscillation T_{23} for the divergent mode of §5.2 as a function of two non-dimensional parameters, $\mu_1 \equiv g(h_{xx}^* - 2D_0/L^2)/B$ and $\mu_2 \equiv f(v_x^* + f)/B$. v_x^* and h_{xx}^* are local extrema in the relative vorticity and free-surface curvature, respectively. The dimensional period of oscillation is $T_{23}/B^{1/2}$.

	B (s^{-2})	A	E	μ_1	μ_2	T_{23}
Case (i)	0.10196×10^{-7}	-2.76909	-1.16331	-0.21167	1.03960	5.59924
Case (ii)	0.29620×10^{-7}	-0.44230	2.42909	-7.28629	0.54018	3.80541
Case (iii)	0.19720×10^{-5}	-0.02538	2.91602	-10.94422	0.03550	3.51437

TABLE 1. Parameter values for case (i) ($L = 10^6$ m), case (ii) ($L = 10^5$ m) and case (iii) ($L = 10^4$ m)

respectively, for 24 periods of the divergent oscillation. Figure 10(*a–c*) depicts the trajectory of a fluid parcel initially located at $(x/L, y/L) = (0.12, 0)$ in cases (i), (ii) and (iii). Figure 10(*d*) shows the trajectory of a fluid element initially located at $(x/L, y/L) = (0.1, 0)$ for a flow scenario similar to that in case (i) but with the Coriolis parameter reduced to $f = 2 \times 10^{-5}$ s^{-1}.

In case (i) the waveforms of the divergent mode functions resemble slightly distorted sinusoids. The crests tend to be slightly flatter than the troughs for the free-surface curvature function, whereas for the relative vorticity the troughs tend to be slightly flatter than the crests. The free-surface curvature is negative throughout the oscillation, indicating that the free surface is always convex (a ridge). Although the relative vorticity is initially positive, it rapidly becomes negative in response to the compression of the absolute vorticity and attains a large negative extremum value at $\tau = \frac{1}{2}T_{23}$. Since the periods of oscillation of the divergent and non-divergent modes are similar ($T_{23} = 5.59924$ and 2π), the non-divergent mode variables appear as amplitude-modulated oscillations with a carrier wave period of T_{23}.

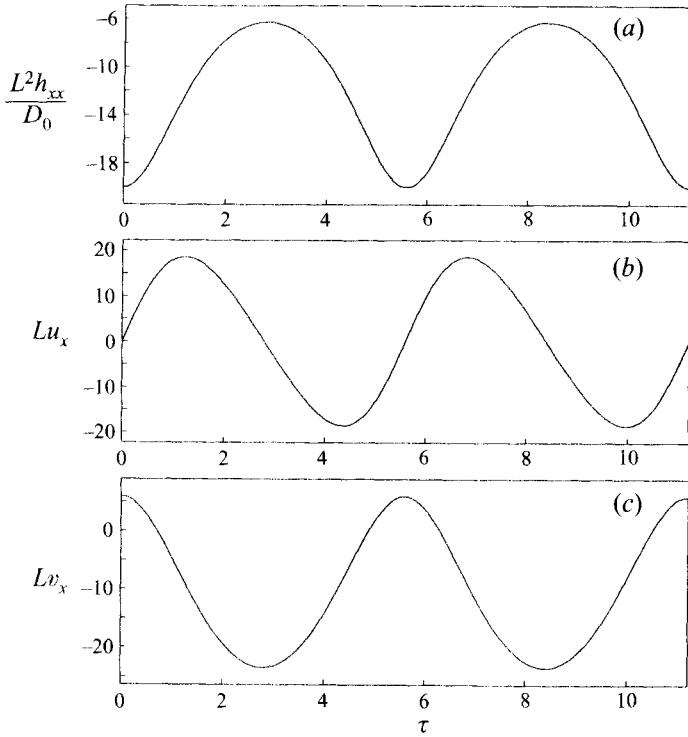In case (ii) the waveforms of the divergent mode functions become quite distorted

FIGURE 4. Time series of the divergent mode functions (a) $L^2 h_{xx}/D_0$, (b) Lu_x and (c) Lv_x for case (i) ($L = 10^6$ m). Two periods of the divergent oscillation are shown. The time τ is non-dimensional. The non-dimensional period is $T_{23} = 5.59924$. The dimensional time is $t = \tau/B^{1/2}$ where $B = 0.10196 \times 10^{-7}$ s^{-2}.

from the sinusoidal form. The free-surface curvature function crests are now much flatter than the troughs and the relative vorticity troughs are much flatter than the crests. The free-surface curvature decreases rapidly in magnitude, becomes positive, and remains slightly positive for over half the period of the oscillation (the fluid ridge collapses rapidly and the free surface becomes slightly concave). The period of oscillation of the divergent mode is no longer similar to that of the non-divergent mode ($T_{23} = 3.80541$ and 2π) and the non-divergent flow variables no longer have a smooth modulated appearance. Instead, some of the variables appear ragged or spiky; more frequencies are apparent and the waveforms are more complicated. Not surprisingly, the shoreline functions and parcel trajectories reveal that the lateral extent of the oscillation (as a fraction of L) is much greater in case (ii) where $L_R/L \sim 1$ (a moderate-rotation regime) than in case (i) where $L_R/L < 1$ (a high-rotation regime).

The shape and amplitude of the divergent mode functions in the low-rotation example, case (iii) ($L_R/L > 1$) are quite similar to the functions in the moderate-rotation example, case (ii) ($L_R/L \sim 1$), with the exception of the relative vorticity which has an amplitude of about half of what it was in case (ii). The non-dimensional period of oscillation of the divergent mode is just slightly smaller in case (iii) ($T_{23} = 3.51437$) than in case (ii) ($T_{23} = 3.80541$). On the other hand, since B is two order of magnitudes larger in case (iii) than in case (ii), the dimensional period ($T_{23}/B^{1/2}$) in case (iii) is an order of magnitude smaller than in case (ii). The waveforms of the non-divergent velocity components in case (iii) are still ragged, but their amplitudes are greatly reduced from those in case (ii). The time average of v_0 for case (iii) (approximately
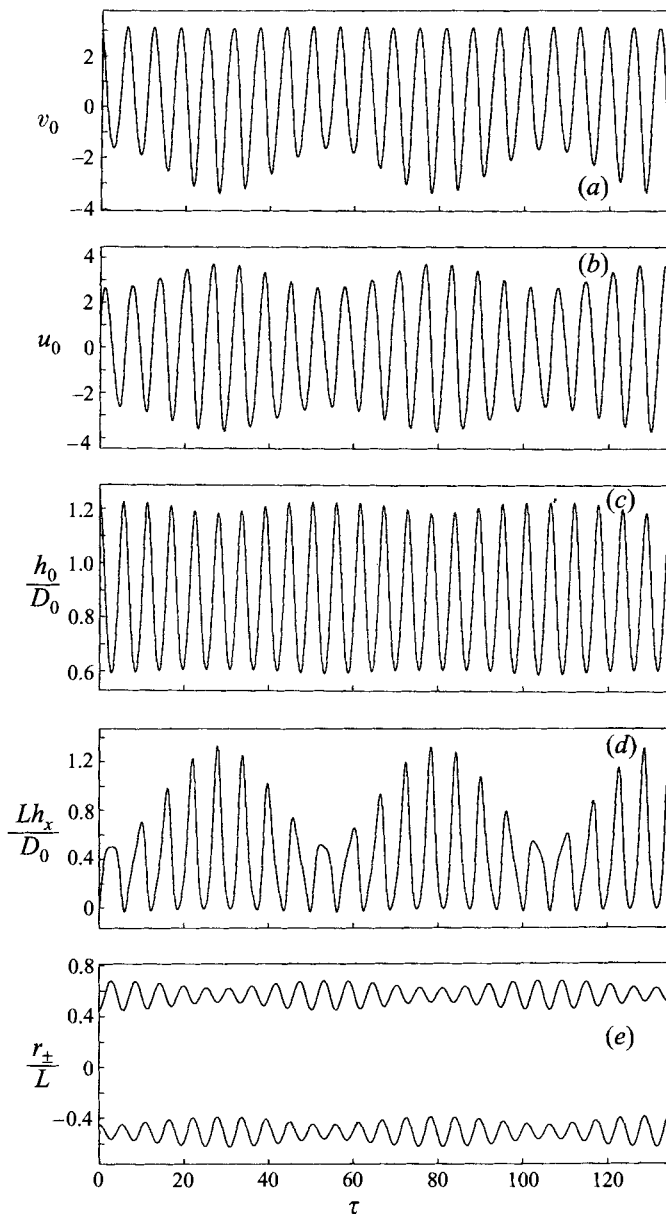
FIGURE 5. Time series of (a) v_0, (b) u_0, (c) h_0/D_0, (d) Lh_x/D_0 and (e) the shoreline functions r_+/L and r_-/L for case (i) ($L = 10^6$ m) for 24 periods of the divergent oscillation. The time τ is non-dimensional. The dimensional time is $t = \tau/B^{1/2}$ where $B = 0.101\,96 \times 10^{-7}$ s^{-2}.

2.9 m s^{-1}) is the largest of the three cases. Because of the relatively large positive mean value of v_0 and lack of negative relative vorticity v_x, the y-component of the sample trajectory in this case is characterized by northward motion. In cases (i) and (ii), the small mean value of v_0 and the presence of negative relative vorticity (which contributes a negative amount xv_x to the total v field for $x > 0$) is associated with southward and northward parcel displacements and loops in the trajectories. We also note that in case (iii) the slope of the free surface at the centreline, h_x, contains both positive and negative spikes (in contrast to the dominant positive spikes in cases (i) and (ii)). These
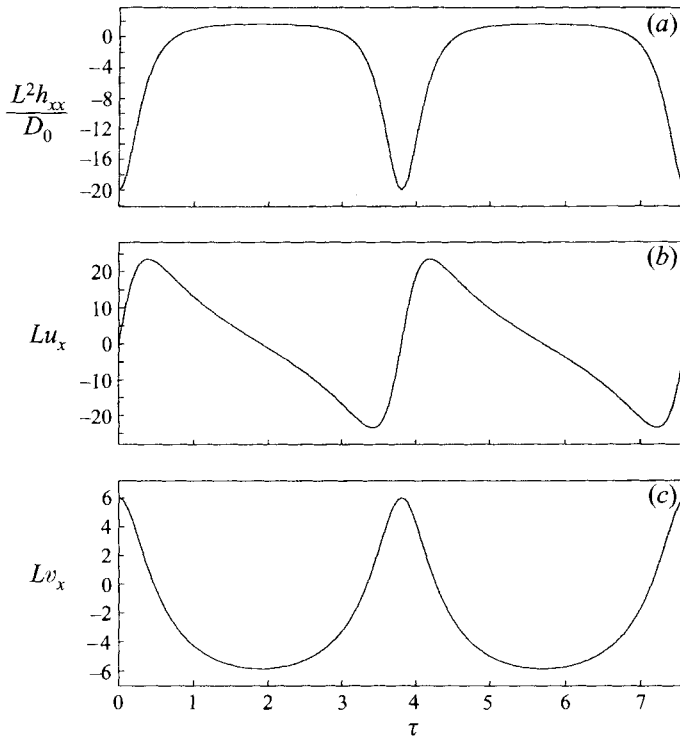
FIGURE 6. As figure 4 but for case (ii) ($L = 10^5$ m); $T_{23} = 3.80541$, $B = 0.29620 \times 10^{-7}$ s^{-2}.

spikes are associated with maxima in the centreline free-surface height h_0, maxima in (convex) free-surface curvature and minima in the distance between the shorelines. Thus, the bulk of the fluid ridge at the time of peak curvature can be to the right or the left of the centreline in case (iii) whereas in cases (i) and (ii) it is primarily to the right of the centreline.

9. Summary

A new exact analytic solution is presented for a class of finite-amplitude inviscid shallow-water oscillations in an infinite straight channel of parabolic depth variation on the rotating Earth. It provides a description of the one-dimensional subclass of flows considered by Ball (1964), Thacker (1981), Cushman-Roisin (1987) and others in which the velocity field varies linearly and the free-surface displacement varies quadratically with the spatial coordinates. The solution is composed of divergent and non-divergent modes. In contrast to the previously derived analytic solutions for flows in elliptic paraboloidal basins, the frequency of the divergent mode for the parabolic channel depends, in part, on the amplitudes of the relative vorticity and free-surface curvature. The flow dependence of this oscillation is an intrinsically nonlinear feature.

Examples were considered of flow in high-, moderate- and low-rotation regimes: $L > L_R$, $L \sim L_R$ and $L < L_R$, respectively. In the high-rotation regime the period of the divergent mode approached that of the non-divergent mode. The waveforms of the non-divergent variables were amplitude modulations of the divergent mode. In the moderate-rotation regime the period of the divergent mode was slightly more than half that of the non-divergent mode. More frequencies were apparent in the waveforms of the non-divergent flow variables and the flow appeared to be quite complex. The non-
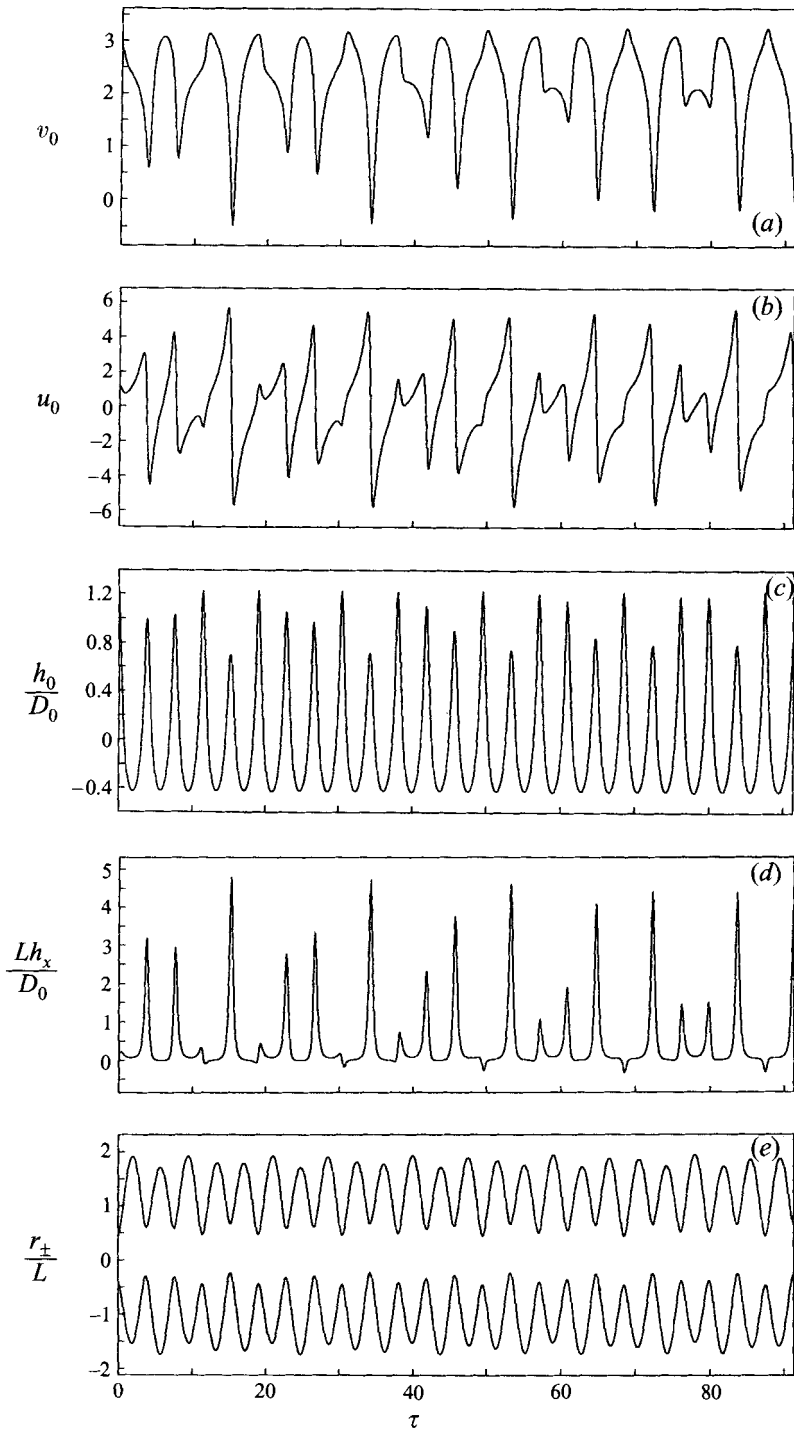
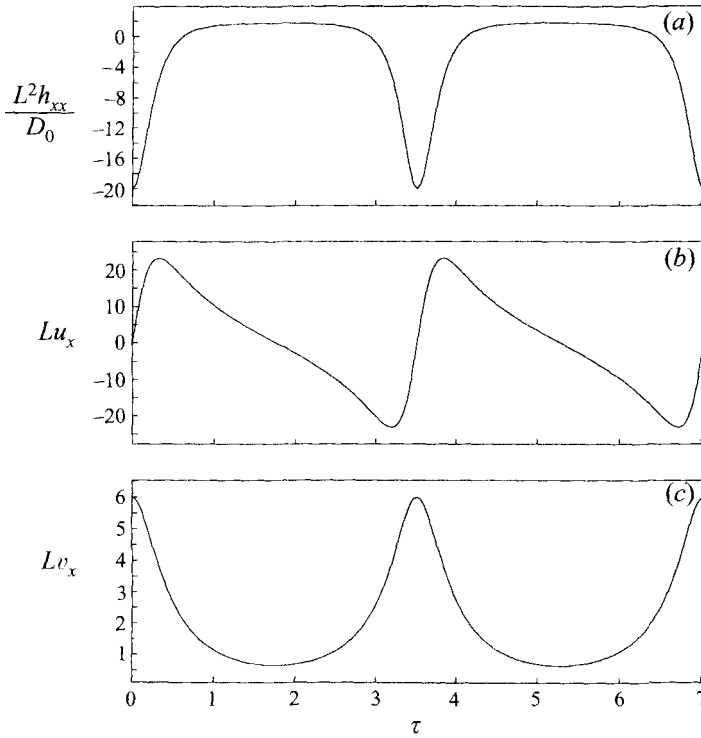FIGURE 7. As figure 5 but for case (ii) ($L = 10^5$ m); $B = 0.29620 \times 10^{-7}$ s^{-2}.

FIGURE 8. As figure 4 but for case (iii) ($L = 10^4$ m); $T_{23} = 3.80541$, $B = 0.19720 \times 10^{-5}$ s^{-2}.

dimensional frequency of the divergent mode in the low-rotation regime was similar to (slightly less than) the frequency in the moderate-rotation regime. As in the moderate-rotation regime, the waveforms of the non-divergent flow variables in the low-rotation regime were also quite complex, though the amplitudes of the oscillations of the velocity functions were of a much smaller amplitude. The behaviour of the sample trajectories (a transition from the closed loops of the high-rotation regime to a northward motion with superimposed lateral oscillations in the low-rotation regime) could be easily interpreted in terms of the behaviour of the velocity functions. Other trajectories (not shown) revealed local and occasionally dramatic sensitivities to the initial location of fluid parcels. It is intriguing that despite the chaotic appearance of some of the variables and trajectories, the analytic flow description involves relatively well-known functions and is exact for all parameter values.

This solution provides a good example of an exact description of nonlinear but non-chaotic behaviour in a simple geophysical system. In addition to representing a fundamental hydrodynamic flow, it can be used as a benchmark test for the validation of numerical shallow-water models and for the determination of optimal computational algo.ithms for systems of nonlinear partial differential equations.
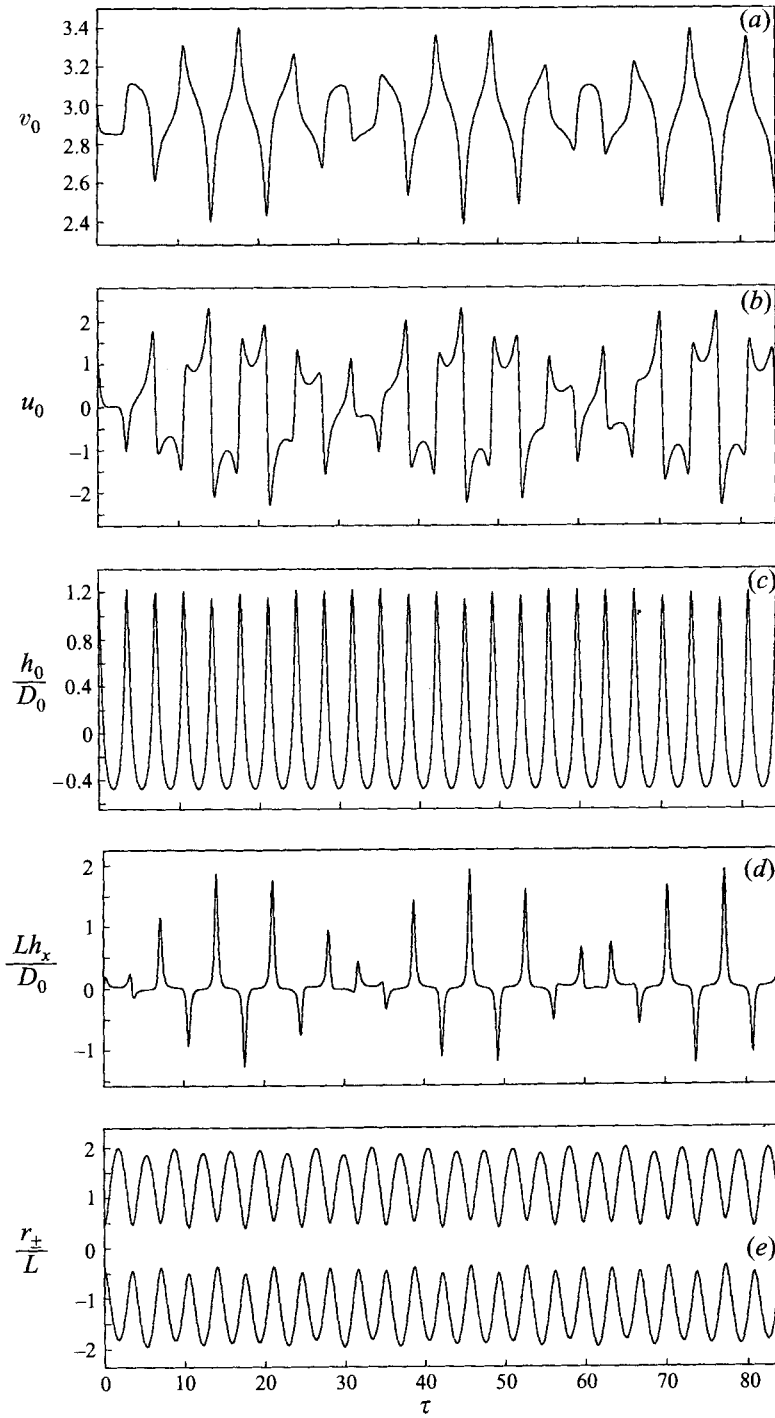
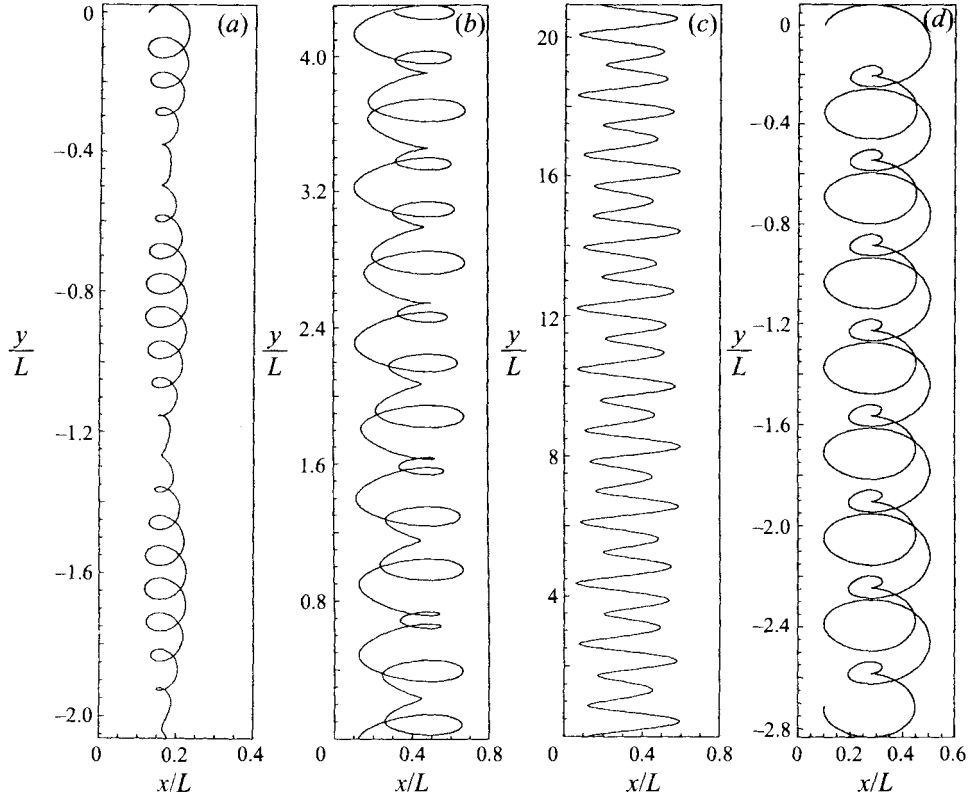FIGURE 9. As figure 5 but for case (iii) ($L = 10^4$ m); $B = 0.19720 \times 10^{-5}$ s^{-2}.

FIGURE 10. Trajectory of a fluid element initially located at $(x/L, y/L) = (0.12, 0)$ in (a) case (i) $(L = 10^6$ m), (b) case (ii) $(L = 10^5$ m) and (c) case (iii) $(L = 10^4$ m). The trajectories are calculated for 24 periods of the divergent oscillation. The net parcel displacement is southward (negative y) in (a) and northward (positive y) in (b) and (c). (d) Trajectory of a fluid element initially located at $(x/L, y/L) = (0.1, 0)$ for a flow scenario similar to that in case (i) but with a reduced Coriolis parameter, $f = 2 \times 10^{-5}$ s^{-1}. The trajectory is calculated for 24 periods of the divergent oscillation. The net parcel displacement is southward (negative y).

Appendix A. Analytic solution of Thacker's (1981) equations (57) and (58)

Thacker's (1981) development of the one-dimensional channel problem led to his equation (57):

$$\frac{d^2 u_x}{dt^2} + 5u_x \frac{du_x}{dt} + 3u_x^3 - 2f u_x v_x + \left(\frac{6gD_0}{L^2} + f^2\right)u_x = 0, \qquad (A\ 1)$$

and to (58) (our (9)), which he solved numerically. To solve the system analytically, we use (23) and the first integral (24) to eliminate u_x and v_x in favour of ϕ:

$$\frac{1}{\phi}\frac{d^3\phi}{dt^3} + \frac{2}{\phi^2}\frac{d\phi}{dt}\frac{d^2\phi}{dt^2} + \frac{3B}{\phi}\frac{d\phi}{dt} - \frac{2af}{\phi^2}\frac{d\phi}{dt} = 0, \qquad B \equiv \frac{2gD_0}{L^2} + f^2. \qquad (A\ 2)$$

Multiplying by the integrating factor ϕ^3 and integrating by parts yields

$$\phi^2 \frac{d^2\phi}{dt^2} + B\phi^3 - af\phi^2 = \text{const.} \qquad (A\ 3)$$

Dividing by ϕ^2 and setting const $= -gc$ yields (26) which is twice integrable.

Appendix B. Roots of $V(\Phi) - E = 0$

If $\Phi^* \neq 0$, the roots of $V(\Phi^*) - E = 0$ (§§5.1 and 5.2) are equivalent to the roots of $\Phi^*[V(\Phi^*) - E] = 0$, that is, the roots of the cubic equation $\Phi^{*3} + a_2 \Phi^{*2} + a_1 \Phi^* + a_0 = 0$, where $a_2 = A$, $a_1 = -E$, and $a_0 = 1$. The three (possibly complex) roots are given by

$$\left.\begin{array}{l} s_1 + s_2 - \tfrac{1}{3}a_2, \\ -\tfrac{1}{2}(s_1 + s_2) - \tfrac{1}{3}a_2 + \tfrac{1}{2}\mathrm{i}\sqrt{3}\,(s_1 - s_2), \\ -\tfrac{1}{2}(s_1 + s_2) - \tfrac{1}{3}a_2 - \tfrac{1}{2}\mathrm{i}\sqrt{3}\,(s_1 - s_2), \end{array}\right\} \tag{B 1}$$

where $s_1 = [r + (q^3 + r^2)^{1/2}]^{1/3}$, $s_2 = [r - (q^3 + r^2)^{1/2}]^{1/3}$, $q \equiv \tfrac{1}{3}a_1 - \tfrac{1}{9}a_2^2$ and $r \equiv \tfrac{1}{6}(a_1 a_2 - 3a_0) - \tfrac{1}{27}a_2^3$ (Abramowitz & Stegun 1964). If $q^3 + r^2 > 0$ there is one real root and a pair of complex-conjugate roots; if $q^3 + r^2 = 0$ all roots are real and at least two are equal, and if $q^3 + r^2 < 0$ all roots are real. It is straightforward to show that the product of the three roots is equal to $-a_0 (= -1)$.

In the present case, $q = -\tfrac{1}{9}(A^2 + 3E)$, $r = -\tfrac{1}{6}(EA + 3) - \tfrac{1}{27}A^3$, and

$$q^3 + r^2 = \tfrac{1}{108}(27 + 18EA - E^2 A^2 + 4(A^3 - E^3)). \tag{B 2}$$

Restricting attention to the real roots, we have, for $q^3 + r^2 > 0$, one real root Φ_1^* given by

$$\Phi_1^* = (r + (q^3 + r^2)^{1/2})^{1/3} + (r - (q^3 + r^2)^{1/2})^{1/3} - \tfrac{1}{3}a_2. \tag{B 3}$$

For $q^3 + r^2 = 0$, there are two real roots Φ_1^* and Φ_2^* given by

$$\Phi_1^* = 2r^{1/3} - \tfrac{1}{3}a_2, \quad \Phi_2^* = -r^{1/3} - \tfrac{1}{3}a_2. \tag{B 4}$$

For $q^3 + r^2 < 0$, there are three real roots Φ_1^*, Φ_2^* and Φ_3^* given by

$$\left.\begin{array}{l} \Phi_1^* = 2(r^2 + |q^3 + r^2|)^{1/6}\cos(\tfrac{1}{3}\theta) - \tfrac{1}{3}a_2, \\ \Phi_2^* = -2(r^2 + |q^3 + r^2|)^{1/6}\cos\tfrac{1}{3}(\theta - \pi) - \tfrac{1}{3}a_2, \\ \Phi_3^* = -2(r^2 + |q^3 + r^2|)^{1/6}\cos\tfrac{1}{3}(\theta + \pi) - \tfrac{1}{3}a_2, \end{array}\right\} \tag{B 5}$$

where

$$\theta = \arccos\left(\frac{r}{(r^2 + |q^3 + r^2|)^{1/2}}\right), \quad \sin\theta \geqslant 0.$$

Appendix C. Evaluation of $I(\Phi_2, \Phi)$

The integral $I(\Phi_2, \Phi)$ appearing in the trajectory calculation of §7.2 is defined by

$$I(\Phi_2, \Phi) = \frac{1}{B^{1/2}} \int_{\Phi_2}^{\Phi} \frac{\Phi'^{3/2}}{[(\Phi' - \Phi_1)(\Phi' - \Phi_2)(\Phi_3 - \Phi')]^{1/2}}\,\mathrm{d}\Phi', \tag{C 1}$$

where $\Phi_3 \geqslant \Phi > \Phi_2 > 0 > \Phi_1$. Changing variables to $\lambda = 1/\Phi$ and making use of the fact that the product of the three roots Φ_1, Φ_2 and Φ_3 is equal to -1 (see Appendix B), we obtain

$$I(\Phi_2, \Phi) = \frac{1}{B^{1/2}} \int_{1/\Phi}^{1/\Phi_2} \frac{1}{\lambda^2 [(\lambda - 1/\Phi_1)(1/\Phi_2 - \lambda)(\lambda - 1/\Phi_3)]^{1/2}}\,\mathrm{d}\lambda, \tag{C 2}$$

where $1/\Phi_2 > \lambda \geqslant 1/\Phi_3 > 0 > 1/\Phi_1$. $I(\Phi_2, \Phi)$ can be reduced to combinations of tabulated integrals by using a reduction formula for elliptic integrals (Abramowitz & Stegun 1964, equation (17.1.5)),

$$y(\lambda - c)^{-s} = (2-s)b_0 J_{s-3} + \tfrac{1}{2}(3 - 2s)b_1 J_{s-2} + (1-s)b_2 J_{s-1} + \tfrac{1}{2}(1-2s)b_3 J_s - sb_4 J_{s+1}, \tag{C 3}$$

where

$$J_s = \int [y(\lambda - c)^s]^{-1} \, d\lambda, \qquad (C\,4)$$

$$y^2 = b_0(\lambda - c)^4 + b_1(\lambda - c)^3 + b_2(\lambda - c)^2 + b_3(\lambda - c) + b_4, \qquad (C\,5)$$

and s is any positive integer. Taking $c = 0$, $s = 1$, $b_0 = 0$, $b_1 = -1$, $b_2 = E$, $b_3 = -A$, and $b_4 = -1$, we get

$$J_2 = \tfrac{1}{2}J_{-1} - \tfrac{1}{2}AJ_1 + \frac{[(\lambda - 1/\Phi_1)(1/\Phi_2 - \lambda)(\lambda - 1/\Phi_3)]^{1/2}}{\lambda}. \qquad (C\,6)$$

$I(\Phi_2, \Phi)$ is proportional to J_2 (with appropriate limits of integration) and we find that

$$I(\Phi_2, \Phi) = \frac{1}{2B^{1/2}} \int_{1/\Phi}^{1/\Phi_2} \frac{\lambda}{[(\lambda - 1/\Phi_1)(1/\Phi_2 - \lambda)(\lambda - 1/\Phi_3)]^{1/2}} \, d\lambda$$

$$- \frac{A}{2B^{1/2}} \int_{1/\Phi}^{1/\Phi_2} \frac{1}{\lambda[(\lambda - 1/\Phi_1)(1/\Phi_2 - \lambda)(\lambda - 1/\Phi_3)]^{1/2}} \, d\lambda$$

$$+ \left[\frac{[(\lambda - 1/\Phi_1)(1/\Phi_2 - \lambda)(\lambda - 1/\Phi_3)]^{1/2}}{\lambda B^{1/2}} \right]_{\lambda = 1/\Phi}^{\lambda = 1/\Phi_2}, \qquad (C\,7)$$

where $1/\Phi_2 > \lambda \geqslant 1/\Phi_3 > 0 > 1/\Phi_1$. Making use of Gradshteyn & Ryzhik (1980, equation (5) of §3.132 and equation (6) of §3.137),† (C 7) becomes

$$I(\Phi_2, \Phi) = \frac{(\Phi_2 - \Phi_1)^{1/2}}{(-B\Phi_1 \Phi_2)^{1/2}} E(\Lambda, P) - \frac{\Phi_2^{1/2}}{[-B\Phi_1(\Phi_2 - \Phi_1)]^{1/2}} F(\Lambda, P)$$

$$- A \frac{\Phi_2(-\Phi_1 \Phi_2)^{1/2}}{[B(\Phi_2 - \Phi_1)]^{1/2}} \Pi \left(\Lambda, 1 - \frac{\Phi_2}{\Phi_3}, P \right) - \frac{[(\Phi - \Phi_1)(\Phi - \Phi_2)(\Phi_3 - \Phi)]^{1/2}}{(B\Phi)^{1/2}}, \quad (C\,8)$$

where

$$\Lambda \equiv \arcsin \left[\frac{\Phi_3 (\Phi - \Phi_2)}{\Phi (\Phi_3 - \Phi_2)} \right]^{1/2}, \qquad P \equiv \left[-\frac{\Phi_1 (\Phi_3 - \Phi_2)}{\Phi_3 (\Phi_2 - \Phi_1)} \right]^{1/2},$$

and $F(\Lambda, P)$, $E(\Lambda, P)$ and $\Pi(\Lambda, 1 - \Phi_2/\Phi_3, P)$ are Legendre elliptic integrals of the first, second and third kinds, respectively.

REFERENCES

ABRAMOWITZ, M. & STEGUN, I. A. 1964 *Handbook of Mathematical Functions with Formulas, Graphs, and Mathematical Tables.* National Bureau of Standards, Washington, DC.

BALL, F. K. 1963 Some general theorems concerning the finite motion of a shallow liquid lying on a paraboloid. *J. Fluid Mech.* **17**, 240–256.

BALL, F. K. 1964 An exact theory of simple finite shallow water oscillations on a rotating earth. In *Hydraulics and Fluid Mechanics* (ed. R. Silvester). Macmillan.

BALL, F. K. 1965 The effect of rotation on the simpler modes of motion of a liquid in an elliptic paraboloid. *J. Fluid Mech.* **22**, 529–545.

CARLSON, B. C. 1979 Computing elliptic integrals by duplication. *Numer. Math.* **33**, 1–16.

CARRIER, G. F. & GREENSPAN, H. P. 1958 Water waves of finite amplitude on a sloping beach. *J. Fluid Mech.* **4**, 97–109.

CUSHMAN-ROISIN, B. 1984 An exact analytical solution for a time-dependent, elliptical warm-core ring with outcropping interface. *Ocean Modelling* **59**, 5–6.

† Equation (5) of §3.132 of Gradshteyn & Ryzhik (1980) contains a misprint, a spurious factor of a/b in the coefficient multiplying the elliptic integral of the second kind.

CUSHMAN-ROISIN, B. 1987 Exact analytical solutions for elliptical vortices of the shallow-water equations. *Tellus* **39A**, 235–244.

CUSHMAN-ROISIN, B., HEIL, W. H. & NOF, D. 1985 Oscillations and rotations of elliptical warm-core rings. *J. Geophys. Res.* **90**, 11756–11764.

DAVIS, H. T. 1962 *Introduction to Nonlinear Differential and Integral Equations.* Dover.

GOLDSBROUGH, G. R. 1931 The tidal oscillations in an elliptic basin of variable depth. *Proc. R. Soc. Lond.* A **130**, 157–167.

GOLDSTEIN, H. 1980 *Classical Mechanics*, 2nd Edn. Addison-Wesley.

GRADSHTEYN, I. S. & RYZHIK, I. M. 1980 *Table of Integrals, Series, and Products.* Academic.

MILES, J. W. & BALL, F. K. 1963 On free-surface oscillations in a rotating paraboloid. *J. Fluid Mech.* **17**, 257–266.

PEDLOSKY, J. 1979 *Geophysical Fluid Dynamics.* Springer.

PRESS, W. H., TEUKOLSKY, S. A., VETTERLING, W. T. & FLANNERY, B. P. 1992 *Numerical Recipes in FORTRAN: The Art of Scientific Computing*, 2nd Edn. Cambridge University Press.

STOKER, J. J. 1958 *Water Waves: The Mathematical Theory with Applications.* John Wiley & Sons.

THACKER, W. C. 1981 Some exact solutions to the nonlinear shallow-water wave equations. *J. Fluid Mech.* **107**, 499–508.

TSONIS, A. A., TRIANTAFYLLOU, G. N., ELSNER, J. B., HOLDZKOM II, J. J. & KIRWAN JR., A. D. 1994 An investigation of the ability of nonlinear methods to infer dynamics from observables. *Bull. Am. Met. Soc.* **75**, 1623–1633.

WHITHAM, G. B. 1974 *Linear and Nonlinear Waves.* John Wiley & Sons.